MODELS OF THE NEAR-SPACE GEOPHYSICAL ENVIRONMENT

Edward C. Robinson
James N. Bass
Krishin H. Bhavnani
Carl A. Hein
William J. McNeil
Douglas S. Reynolds

30 June 1997

19980102 005
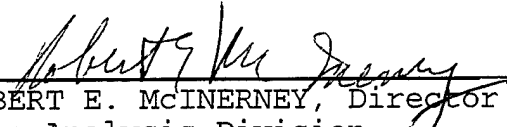
PHILLIPS LABORATORY
Directorate of Geophysics
AIR FORCE MATERIEL COMMAND
HANSCOM AIR FORCE BASE, MA 01731-3010

"This technical report has been reviewed and is approved for publication"

EDWARD C. ROBINSON
Contract Manager
Data Analysis Division

ROBERT E. McINERNEY, Director
Data Analysis Division

This report has been reviewed by the ESD Public Affairs Office
(PA) and is releasable to the National Technical Information
Service (NTIS).

Qualified requestors may obtain additional copies from the Defense
Technical Information Center. All others should apply to the
National Technical Information Service.

If your address has changed, or if you wish to be removed from the
mailing list, or if the addressee is no longer employed by your
organization, please notify PL/IM, 29 Randolph Road, Hanscom AFB, MA
01731-3010. This will assist us in maintaining a current mailing list.

Do not return copies of this report unless contractual obligations or
notices on a specific document requires that it be returned.

REPORT DOCUMENTATION PAGE

1. AGENCY USE ONLY (Leave Blank)	2. REPORT DATE 30 June 1997	3. REPORT TYPE AND DATES COVERED Scientific Interim

4. TITLE AND SUBTITLE

Models of the Near-Space Geophysical Environment

5. FUNDING NUMBERS
PE 62601F
Project 1010
Task GZ Work Unit 00

6. AUTHORS

E. C. Robinson	J. N. Bass*	K. H. Bhavnani*
C. A. Hein*	W. J. McNeil*	D. S. Reynolds*

7. PERFORMING ORGANIZATION NAME(S) AND ADDRESS(ES)

Phillips Laboratory
29 Randolph Road
Hanscom AFB, MA 01731-3010

8. PERFORMING ORGANIZATION REPORT NUMBER

PL-TR-97-2089
ERP, No. 1207

9. SPONSORING / MONITORING AGENCY NAME(S) AND ADDRESS(ES)

10. SPONSORING / MONITORING AGENCY REPORT NUMBER

11. SUPPLEMENTARY NOTES

*Radex, Inc.
3 Preston Court   Partially funded by Contract F19628-93-0023
Bedford, MA 01730

12a. DISTRIBUTION / AVAILABILITY STATEMENT

Approved for Public Release
Distribution Unlimited

12b. DISTRIBUTION CODE

13. ABSTRACT (Maximum 200 words)

This report provides descriptions of environmental models used in the near-earth environment for the analysis of earth-based and satellite data. Included are models of the ionosphere, atmosphere, radiation belt, Earth's magnetic field, and orbital prediction. These models are used at PL for a variety of purposes, in particular, for the analysis of experimental data obtained from ground based instruments and, where applicable, instruments carried on balloons, rockets, and satellites. Some of the models described here were developed at PL based upon such measurements. For many of the models described here, computer output is provided together with estimates of computer (CPU) times required to generate such output. The computer codes (subroutines) for these models are frequently incorporated into programs used for data analysis and reduction, as well as mission planning. It is hoped that this report will serve as a useful reference for planning such future missions.

14. SUBJECT TERMS Ionosphere models, Ionosphere ray tracing, Radiation belt flux and dose models, Magnetic field models, Corrected geomagnetic coordinates, Atmospheric models, Orbital prediction models

15. NUMBER OF PAGES

16. PRICE CODE

17. SECURITY CLASSIFICATION OF REPORT Unclassified	18. SECURITY CLASSIFICATION OF THIS PAGE Unclassified	19. SECURITY CLASSIFICATION OF ABSTRACT Unclassified	20. LIMITATION OF ABSTRACT Unlimited

Contents

Preceding Page Blank

Tables

Acknowledgements

Models of The Near-Space Geophysical Environment

1. INTRODUCTION

This report provides descriptions of environmental models used in the near-earth environment for the analysis of earth-based and satellite data. Included are models of the ionosphere, atmosphere, radiation belt, Earth's magnetic field, and orbital prediction. These models are used at PL for a variety of purposes, in particular, for the analysis of experimental data obtained from ground based instruments and, where applicable, instruments carried on balloons, rockets, and satellites. Some of the models described here were developed at PL based upon such measurements. Extensive literature exists describing the scientific background of the models. The *Handbook of Geophysics and the Space Environment* [Jursa, 1985] is in particular pertinent to PL and this report, but clearly shows that many models remain to be documented. For many of the models described here, computer output is provided together with estimates of computer (CPU) times required to generate such output. The computer codes (subroutines) for these models are frequently incorporated into programs used for data analysis and reduction, as well as mission planning. It is hoped that this report will serve as a useful reference for planning such future missions. Although most of the programs are in the public domain, some of the ionospheric and radiation belt models are developed and distributed by the PL research branches.

2. IONOSPHERE MODELS AND IONOSPHERE RAY TRACING

This section provides a description of several ionospheric models, which provide empirical and mathematical representations of the electron density of the ionosphere, and, in some cases, density of ions, electron and ion temperatures for a variety of conditions ranging from magnetically quiet, to active conditions. Some of the models provide estimates of ionospheric propagation conditions based upon solar activity, which can be used as the basis of ionospheric ray tracing routines. Descriptions of two ray tracing routines are also provided.

2.1 International Reference Ionosphere 1990 (IRI-90)

The International Reference Ionosphere (IRI) [*Bilitza*, 1990] is the empirical reference model of ionospheric densities and temperatures (electrons and ions) recommended for international use by the Committee on Space Research (COSPAR) and the International Union of Radio Science (URSI). IRI was established in a world-wide collaborative effort beginning in the late sixties, and is updated bi-yearly during special workshops.

IRI is based on both ground-based (ionosonde, absorption, and incoherent scatter) and spacecraft measurements (Alouette, ISIS, AE, AEROS, DE, and rockets). The model provides monthly mean values for magnetically quiet conditions at non-auroral latitudes, for altitudes ranging from 50 km to 2000 km. This model serves as a standard reference for various purposes, such as design of experiments, estimation of environmental and other effects, and testing theories. IRI calculates electron density, electron and ion temperatures, and the composition of positive ions. It computes the density for atomic ions O^+, H^+, He^+, and for molecular O_2^+ and NO^+.

IRI-90 offers several new options not found in its predecessor, IRI-86:

- URSI-1989 foF2 model
- Gulyaeva-1987 model for F2 bottomside thickness
- Analytical LAY-representation of E-F region
- Danilov-Yaichnikov-1985 model for ion composition

A significant improvement in the representation of the foE nighttime variation has been incorporated in IRI-90. In addition, the neutral temperature is obtained with CIRA-86, rather than with CIRA-72.

IRI will produce profiles in latitude or longitude (geodetic or geomagnetic), solar activity, month, day of year, local (or universal) time, or altitude. The user must supply latitude, longitude, sunspot number, and time. Calculation of the full set of output parameters for a profile containing 9000 points requires 20 seconds on a 66 MHz 486 PC. Table 1 shows a sample IRI profile for 12 UT on October 15, at 42.5°N and -71.3°E, with a sunspot number of 100.

Table 1. Sample IRI-90 Output

H(KM)	ELECTRON DENSITY NE/CM-3	NE/NMF2	TEMPERATURES TN(K)	TI(K)	TE(K)	TE/TI	ION PERCENTAGE DENSITIES O+	H+	He+	O2+	NO+
100.0	53912	.0936	-1	-1	-1	-1.00	0	0	0	24	76
200.0	218473	.3794	874	874	1391	1.59	73	0	0	3	24
300.0	553447	.9612	960	1036	2370	2.29	100	0	0	0	0
400.0	365041	.6340	969	1199	2789	2.33	100	0	0	0	0
500.0	199534	.3465	971	1401	2651	1.89	96	4	0	0	0
600.0	117433	.2040	971	1620	2511	1.55	88	10	1	0	0
700.0	81118	.1409	971	1840	2598	1.41	80	18	2	0	0
800.0	64534	.1121	971	2059	2728	1.32	69	28	3	0	0
900.0	56538	.0982	971	2279	2858	1.25	59	37	4	0	0
1000.0	52521	.0912	971	2498	2989	1.20	50	45	5	0	0

```
I-URSI --B0Gul-----------I---------------------I----------------------I
LAT/LON= 42.5/-71.3    H=1000.0  RZ12=100.0 MMDD:1015  LT: 7.2  SZA= 80.2
MLA/MLO= 53.8/358.2  DIP= 71.4  F10.7=145.4  DDD: 288  UT:12.0  SDE= -9.1
```

2.2 The Ionospheric Communications Analysis And Prediction Program (IONCAP)

IONCAP [*Lloyd, et al.*, 1982] is an improved, more versatile and flexible version of the ITS-78 model [*Barghausen, et al.*, 1978]. IONCAP is most useful for wave propagation using operating frequencies that may be reflected by the E, Es, F1, and F2 layers. It is designed mainly for quiet ionospheric conditions. IONCAP does not include the mid-latitude trough, which exhibits large horizontal gradients in electron density, and does not take into account the effects of particle precipitation in the auroral region. The model is good for $\pm20°$ to $\pm60°$, but is a poor predictor for the equatorial region and the high latitude region.

The ITS-78 model was developed by the Institute of Telecommunication Sciences, ESSA, Boulder, Colorado, primarily for the purpose of predicting long term performance of communication systems in the 2 to 30 MHz frequency range. The important features of ITS-78 are the parameters for the D, E, Es, and F2 layers of the ionosphere. IONCAP contains several significant improvements over ITS-78 [*Dandekar*, 1982]:

- The description of the ionosphere is more complete.
- The loss equations were supplemented.
- Ray path geometry calculations were revised.
- Loss statistics were revised to include the effects of the sporadic E layer and of over-the-MUF (maximum usable frequency) modes.
- A separate long path model was developed
- The antenna gain package was revised.

IONCAP has thirty output options, which may be divided into four categories: ionospheric description, antenna patterns, MUF predictions, and system performance predictions. Program inputs are the date, universal time, geographic locations of the transmitter and receiver, and sunspot number. For system performance, some additional inputs are required, such as radiation power of the transmitter, and the signal-to-noise ratio of the receiver. External ionospheric parameters may also be given.

Table 2 shows some sample IONCAP output for points along a great circle path from Denver to St. Louis. A full IONCAP test run required 30 seconds on a 66 MHz 486 PC.

Table 2. Sample IONCAP Output

```
          JAN     1970            SSN = 100.
   BOULDER,COLORADO  TO ST. LOUIS,MO.          AZIMUTHS           N. MI.      KM
   40.03 N  105.30 W - 38.67 N    90.25 W     91.84  281.42      702.6   1301.1

              YE =  20.0     HE = 110.0     HS = 110.0
```

LAT	LONG	LMT	UT	E	F1	Y1	H1	FH/2	F2Z	Y2
H2	ES	MED	HI	M3000	HPF2	RAT	ZEN	ZMAX	MAGL	
39.6N	97.7W	1.5	8.0	.58	.0	.0	.0	.7	4.4	70.3
325.4	1.3	1.8	4.0	2.97	325.7	4.6	154.7	66.1	49.4N	
39.6N	97.7W	3.5	10.0	.61	.0	.0	.0	.7	4.1	75.6
338.9	1.1	1.7	3.5	2.89	339.3	4.5	132.9	66.1	49.4N	
39.6N	97.7W	5.5	12.0	1.02	.0	.0	.0	.7	3.4	82.2
335.8	1.2	1.7	3.5	2.90	337.8	4.1	109.9	66.1	49.4N	
39.6N	97.7W	7.5	14.0	1.95	.0	.0	.0	.7	6.0	85.4
298.3	1.8	2.1	3.9	3.13	300.5	3.5	88.7	66.1	49.4N	
39.6N	97.7W	9.5	16.0	2.93	.0	.0	.0	.7	9.3	93.7
279.2	2.6	2.9	4.4	3.26	281.3	3.0	71.7	66.1	49.4N	
39.6N	97.7W	11.5	18.0	3.44	4.5	51.4	205.5	.7	10.9	105.7
287.9	3.1	3.4	4.4	3.16	295.0	2.7	63.0	66.1	49.4N	
39.6N	97.7W	13.5	20.0	3.28	.0	.0	.0	.7	11.5	99.5
304.2	2.9	3.2	4.0	3.09	305.9	3.1	66.1	66.1	49.4N	
39.6N	97.7W	15.5	22.0	2.43	.0	.0	.0	.7	10.8	91.0
301.4	2.2	2.5	3.5	3.11	302.4	3.3	79.6	66.1	49.4N	
39.6N	97.7W	17.5	.0	1.38	.0	.0	.0	.7	8.7	81.6
299.2	1.5	1.9	3.5	3.13	299.7	3.7	99.1	66.1	49.4N	
39.6N	97.7W	19.5	2.0	.74	.0	.0	.0	.7	6.0	74.7
304.5	1.2	1.7	3.9	3.10	304.8	4.1	121.5	66.1	49.4N	
39.6N	97.7W	21.5	4.0	.55	.0	.0	.0	.7	4.3	71.6
318.7	1.3	1.7	4.4	3.01	319.0	4.5	144.4	66.1	49.4N	
39.6N	97.7W	23.5	6.0	.56	.0	.0	.0	.7	3.8	70.2
325.6	1.4	1.8	4.4	2.97	326.0	4.6	162.3	66.1	49.4N	

2.3 Fully Analytic Ionospheric Model (FAIM)

The Fully Analytic Ionospheric Model (FAIM) [*Anderson, et al.*, 1989] was designed to improve over IONCAP in the equatorial region. FAIM was created by merging a modified version of the Ching-Chiu model [*Chiu*, 1975] with a semiempirical low-latitude ionospheric model (SLIM) [*Anderson, et al.*, 1987].

Some of the FAIM features, such as the post-sunset rise in the F layer peak height, and the equatorial anomaly maxima in plasma density near ±15° geomagnetic latitude, were designed to approximate those in SLIM. The implementation of these features provides significant improvements over previous comparable analytic models.

The FAIM model will generate profiles of NO^+, O_2^+, O^+, and total ion density at one hour increments of local time. These profiles may be easily interpolated to any arbitrary universal time. As distributed, FAIM provides the profiles over an altitude range of 90 km to 1000 km, at 10 km intervals, although densities may also be calculated for any arbitrary altitude within this range. FAIM is valid only for geomagnetic latitudes between -40° and 40°. Seasonal variation is controlled by specifying a month for the run; no day number may be given. FAIM has been superseded by PIM, mainly due to this latitude restriction.

The sample FAIM output shown in Table 3 was generated for October, 0 UT, for a flux of 150. The ion densities have been converted to electron frequency using the relation FREQ = SQRT (DEN/12.4). Electron frequencies are shown for eight locations along a great circle path originating from Bangor, Maine. A more extensive test run on a 40 MHZ Sparc IPX workstation using 92 altitude points, 24 local times, and 17 latitude/longitude pairs required 79 seconds.

Table 3. Sample FAIM Output

Lat	35.8	26.8	17.8	8.8	-0.2	-9.2	-18.2	-27.2
Long	292.2	292.2	292.2	292.2	292.2	292.2	292.2	292.2
Range	1000	2000	3000	4000	5000	6000	7000	8000
1000.	0.402	0.492	0.852	1.529	3.626	4.836	4.902	2.965
900.	0.696	0.852	1.448	2.524	5.529	6.611	6.927	4.701
800.	1.136	1.391	2.393	4.145	8.309	8.785	9.559	7.432
700.	1.796	2.236	3.863	6.684	12.045	11.050	12.508	11.486
600.	2.797	3.570	6.150	10.503	16.072	12.440	14.660	16.841
500.	4.183	5.448	9.333	15.303	17.579	10.821	13.314	21.540
400.	5.658	7.465	12.527	18.217	10.962	5.016	6.312	18.766
300.	5.896	7.389	11.238	10.140	1.555	0.635	0.751	4.803
200.	1.656	1.606	1.727	0.751	0.635	0.635	0.635	0.751
100.	0.635	0.635	0.696	0.696	0.696	0.696	0.696	0.751

2.4 Parameterized Ionospheric Model (PIM)

The Parameterized Ionospheric Model (PIM) [*Whartenby*, 1993] is the base ionospheric model on which the Parameterized Real-time Ionospheric Specification Model (PRISM) [*Daniell, et al.*, 1995] operates. PRISM uses data from ground-based and satellite-based sources to adjust the parameterized model, giving a near real-time specification of the ionosphere. PIM is in the public domain and is available for distribution to the ionospheric community.

PIM is based on four physical models:

- A low-latitude F layer model (LOWLAT) [*Anderson*, 1973].
- MIDLAT, a mid-latitude version of LOWLAT.
- An E-region local chemistry code (ECSD) incorporating photoelectrons using the continuous slowing down method [*Jasperse*, 1982].
- The Time Dependent Ionospheric Model (TDIM) of Utah State University (USU), a high latitude E and F layer model [*Schunk*, 1988].

All of these models use the MSIS-86 thermospheric model [*Hedin*, 1987], and are based on a tilted dipole representation of the geomagnetic field and a corresponding magnetic coordinate system. PIM is an improvement over IONCAP because it provides much better results in the equatorial region, mainly due to the inclusion of a neutral wind model. In addition, PIM considers magnetic activity, rather than assuming average conditions.

PIM may produce either regional or global output; the latitude/longitude grid is user selectable. The model is valid over an altitude range of 90 to 1000 km. The following types of output may be generated:

- Electron density profiles
- Critical frequencies and heights of the E and F_2 layers
- Critical frequencies and heights, plus topside density and scale height, and bottomside densities.

The sample PIM output shown in Table 4 was generated for 1991, day 354, 21 UT, with a fixed latitude of 40°. The Sun Spot Number was given as 130, and K_p was set at 2. The left column indicates altitude, in kilometers; east longitude is shown across the top. A test run on a 40 MHz Sparc IPX workstation calculating electron density profiles for 92 altitude points and 120 latitude /longitude pairs required 106 seconds.

Table 4. Sample PIM Output

	0°	60°	120°	180°	240°	300°
100	3.89E+03	8.95E+02	2.88E+02	2.68E+03	1.31E+05	1.16E+03
200	2.06E+03	2.59E+03	2.83E+03	5.18E+05	5.05E+05	1.95E+04
300	3.08E+05	2.22E+05	1.81E+05	9.65E+05	1.11E+06	7.79E+05
400	4.16E+05	5.60E+05	3.13E+05	4.12E+05	4.97E+05	5.60E+05
500	2.21E+05	2.95E+05	1.69E+05	1.98E+05	2.41E+05	3.04E+05
600	1.06E+05	1.28E+05	8.02E+04	1.12E+05	1.35E+05	1.70E+05
700	5.47E+04	5.69E+04	4.00E+04	7.46E+04	8.98E+04	1.11E+05
800	2.92E+04	2.62E+04	2.06E+04	5.20E+04	6.22E+04	7.48E+04
900	1.60E+04	1.23E+04	1.08E+04	3.73E+04	4.44E+04	5.21E+04
1000	8.97E+03	5.95E+03	5.81E+03	2.72E+04	3.22E+04	3.70E+04

2.5 General Electric Over-the-Horizon (GE/OTH) Ionospheric Model

The General Electric Over-the-Horizon (GE/OTH) model is a revision of the AFGWC polar model [*AFGWC*, 1982], developed by the U.S. Air Force Global Weather Central. This model, also known as the AN/FPS 118 - Analytical Model Specification [*Millman, et al.*, 1988], was developed for frequency management of the Over-the-Horizon Backscatter (OTH-B) radar, and for target coordinate registration and propagation assessments.

The GE/OTH model uses the ITS-78 ionospheric model [*Barghausen*, 1978] as a starting point. The basic model is driven by an effective sunspot number computed from foF_2 data for the past 5 days from a network of 50 ionospheric stations. Using K_p and the effective auroral oval parameter Q_E, the auroral E and F layer enhancements and the mid-latitude F layer trough electron density depletion are superposed on the ITS-78 model. Ionospheric parameters obtained by the automated Air Weather Service (AWS) Digital Ionospheric Sounding System (DISS) network are used for real-time updating of the model at the radar sites.

The software for the GE/OTH model is somewhat more complicated than that of other ionospheric models. Presently, the program is available only for the VAX/VMS operating system. Two separate connections are required - a "master" program, which runs the actual model, and a "driver", which provides the user interface. The two processes are linked through interprocess communication and a shared memory area. A full program run takes approximately 90 seconds on a VAX 7000.

The GE/OTH model requires a "grid" file containing a series of latitude/longitude pairs. The user must provide K_p, Q, sunspot number, date, and time; these values are entered through the driver program. Table 5 presents some typical output from the GE/OTH model. The ground points were traced along a 170° azimuth from the East Coast Radar System (ECRS) in Bangor, Maine. The run was made for December 20, 1992, using K_p and Q of 2, and a sunspot number of 75.

7

Table 5. Sample GE/OTH Model Output

Range	GGLAT	GGLON	GMLAT	GMLON	foF2	HmF2	YmF2	foF1	HmF1	YmF1	foE	HmE	YmE
16	44.8	292.0	55.9	10.0	4.10	317.9	69.3	0.00	0.0	0.0	0.60	120.0	21.8
998	35.9	293.9	46.9	11.2	4.27	318.4	69.1	0.00	0.0	0.0	0.60	120.0	21.8
1999	27.0	295.4	38.0	11.7	4.35	318.0	75.3	0.00	0.0	0.0	0.60	120.0	21.8
3000	18.1	296.6	29.3	11.8	4.64	315.7	79.6	0.00	0.0	0.0	0.60	120.0	21.8
4001	9.1	297.8	20.9	11.6	6.35	312.1	80.9	0.00	0.0	0.0	0.60	120.0	21.8
5001	0.2	298.9	12.6	11.3	10.15	314.1	83.1	0.00	0.0	0.0	0.60	120.0	21.8
6002	-8.7	300.0	4.3	10.9	9.69	345.7	91.5	0.00	0.0	0.0	0.60	120.0	21.8
7003	-17.6	301.1	-5.1	10.6	9.06	388.2	102.9	0.00	0.0	0.0	0.60	120.0	21.8
8004	-26.6	302.4	-13.9	10.6	10.02	385.2	103.3	0.00	0.0	0.0	0.60	120.0	21.8
9005	-35.5	303.9	-22.3	11.2	8.99	375.2	103.8	0.00	0.0	0.0	0.60	120.0	21.8
10005	-44.4	305.7	-30.5	12.4	8.55	369.2	105.1	1.01	231.5	57.9	0.60	120.0	21.8
11006	-53.2	308.2	-38.7	14.5	8.20	350.0	98.5	2.49	227.4	56.9	1.83	120.0	21.8
12007	-62.0	312.1	-47.0	17.5	7.50	330.5	92.4	3.65	223.3	55.8	2.34	120.0	21.8
13008	-70.6	319.0	-55.4	21.8	6.65	310.2	90.1	4.00	219.2	54.8	2.64	120.0	21.8

2.6 The RAYLAB Ray Tracing Program

RAYLAB is a two-dimensional ray tracing program developed by Chris Coleman of the Australian Defence Science and Technology Organization (DSTO). RAYLAB was developed concurrently with HASEL [*Coleman*, 1993], a three-dimensional ray tracing program.

A two-dimensional ray trace assumes that the rays are confined to a fixed azimuthal path emanating from the radar. Three-dimensional models more closely approximate actual ray behavior; however, the "drift" in and out of the azimuthal plane is generally small compared to the distance traveled from the radar. The two-dimensional model may be constructed with a substantially reduced set of equations, resulting in a significant increase in program speed.

RAYLAB is designed to ray trace in an ionosphere with a spatially varying electron density. A Runge-Kutta-Fehlberg scheme is used to solve a simplified version of the Haselgrove form of the ray equations. In essence, this procedure is a simplified version of the technique used in HASEL. Two slightly different versions of RAYLAB have been distributed. One uses a simple Chapman layer ionospheric model, while the other incorporates the FAIM model. In addition, a third version has been adapted to use ionospheric predictions from PIM.

A portion of the output from a typical RAYLAB run is shown in Table 6. The ionosphere was generated with PIM, for 1991, day 354, 1 UT, with a Sunspot Number of 109.4 and K_p of 2. Rays were traced along a 110° azimuth from Bangor, Maine (44.8° N, -68° E), at a frequency of 10 MHz. The data given in the table show altitude and range for a ray with a starting elevation of 4°, out to a range of 6000 km. The complete run, calculating rays for 16 different starting elevations, required 1.06 seconds on a Silicon Graphics workstation equipped with a 150 MHZ R4400 processor.

8

Table 6. Sample RAYLAB Output

Alt	Range	Alt	Range	Alt	Range	Alt	Range
0.0	0.0	248.8	1538.7	6.4	3089.6	134.8	4626.8
3.7	49.8	242.2	1585.0	4.7	3139.5	145.0	4674.6
7.8	99.6	232.6	1631.5	3.3	3189.5	155.5	4722.4
12.2	149.4	221.0	1678.1	2.4	3239.5	166.3	4769.9
17.1	199.0	208.8	1724.9	1.9	3289.4	177.4	4817.3
22.3	248.6	196.6	1771.9	1.7	3339.4	188.8	4864.6
27.9	298.1	184.8	1819.0	1.9	3389.4	197.0	4898.4
33.9	347.5	173.4	1866.3	2.6	3439.4	204.1	4928.4
40.3	396.8	162.3	1913.8	3.6	3489.4	209.2	4952.1
47.1	446.0	151.7	1961.4	5.0	3539.3	214.0	4979.0
54.2	495.1	141.4	2009.2	6.8	3589.2	217.3	5005.6
61.8	544.1	131.5	2057.1	9.0	3639.1	218.7	5035.3
69.7	592.9	122.0	2105.2	11.6	3689.0	216.2	5082.5
78.0	641.7	112.7	2153.4	14.5	3738.8	209.4	5129.8
86.7	690.3	103.6	2201.8	17.9	3788.5	200.8	5177.3
89.9	708.0	95.0	2250.3	21.7	3838.2	192.0	5224.9
95.5	737.6	86.7	2298.9	25.8	3887.9	183.4	5272.7
104.8	785.9	78.8	2347.6	30.3	3937.5	175.2	5320.6
114.5	834.1	71.3	2396.5	35.2	3987.0	167.4	5368.7
124.6	882.2	64.2	2445.5	40.5	4036.4	160.0	5416.8
135.0	930.1	57.4	2494.5	46.2	4085.7	152.9	5465.1
145.8	977.8	51.0	2543.7	52.3	4135.0	146.2	5513.4
156.9	1025.4	45.1	2593.0	58.7	4184.1	139.9	5561.9
168.3	1072.8	39.4	2642.3	65.6	4233.2	133.7	5610.4
180.0	1120.1	34.2	2691.8	72.8	4282.1	127.8	5659.1
192.2	1167.1	29.4	2741.3	80.4	4331.0	122.3	5707.8
204.7	1214.0	24.9	2790.9	88.3	4379.7	117.1	5756.6
217.3	1260.8	20.9	2840.6	90.8	4394.1	112.4	5805.4
229.3	1307.3	17.2	2890.3	99.3	4442.6	108.2	5854.4
239.6	1353.7	13.9	2940.0	106.4	4482.3	104.5	5903.4
247.2	1400.0	11.0	2989.9	115.5	4530.6	101.0	5952.4
251.3	1446.3	8.5	3039.7	125.0	4578.8	97.6	6001.5
251.9	1492.5						

2.7 The HASEL Ray Tracing Program

HASEL [*Coleman*, 1993] is a three-dimensional ray tracing program developed by Chris Coleman of the Australian Defence Science and Technology Organization (DSTO). HASEL was developed concurrently with RAYLAB, a two-dimensional ray tracing program.

Unlike a two-dimensional ray trace, which assumes that the rays are confined to a fixed azimuthal path, three-dimensional models closely approximate actual ray behavior. Consequently, the three-dimensional model is constructed with a much more complex set of equations, resulting in a significant increase in program run-time.

The procedure is based on a numerical solution to the Haselgrove ray tracing equations. These are ordinary differential equations, which are solved using a Runge-Kutta-Fehlberg scheme. The Earth's magnetic field is represented by a tilted dipole. There are three options for representing the ionosphere:

• The ionosphere can be defined using an internal function subroutine, ELDEN. This is a simple analytic ionospheric model.

• A description of the ionosphere may be given in terms of layer parameters, defined on a regular (that is, even increments) geographic latitude/longitude grid. The three layers (E, F_1, and F_2) are defined by their heights, plasma frequencies at these heights, and layer thicknesses. The electron density profile is then composed of Chapman layers.

• The third option is similar to the previous method, but the Chapman layers are replaced with a set of samples above each geographical grid point. As with the geographic sampling, the altitude sampling must also be uniform; a three-dimensional interpolation scheme is then used to determine electron densities. This is the most efficient of the three ionospheric representations.

A portion of the output from a typical HASEL run is shown in Table 7. This ray trace was made using the ELDEN function to represent the ionosphere, with the magnetic field effects active, and medium tolerance. Rays were evaluated for all combinations of four bearings, six initial elevation angles, and three frequencies. The complete run required 66 seconds on a Silicon Graphics workstation equipped with a 150 MHZ R4400 processor.

Table 7. Sample HASEL Output

Doppler Shift	Ground Range	Group Path	Phase Path	Max Height	Init Elev	Final Elev	Final Long	Final Lat	Bear	Freq	Mode
-0.84	1882.2	1975.7	1956.3	219.3	10.0	10.0	295.3	28.1	170.0	10.0	F2O
-1.69	3769.4	3956.3	3917.6	219.5	10.0	9.9	297.7	11.3	170.0	10.0	F2OF2O
-1.68	3751.4	3938.0	3898.8	217.2	10.0	10.0	297.6	11.4	170.0	10.0	F2OF2
-2.53	5642.5	5922.7	5864.2	217.1	10.0	9.9	299.8	-5.4	170.0	10.0	F2OF2OF2X
-2.53	5661.0	5941.6	5883.6	219.5	10.0	9.9	299.8	-5.6	170.0	10.0	F2OF2OF2O
-2.52	5622.7	5902.6	5843.5	217.2	10.0	10.0	299.7	-5.2	170.0	10.0	F2OF2XF2X
-2.53	5641.2	5921.5	5862.9	219.6	10.0	9.9	299.8	-5.4	170.0	10.0	F2OF2XF2O
-0.84	1865.7	1958.8	1939.0	217.3	10.0	10.0	295.3	28.2	170.0	10.0	F2X
-1.69	3749.7	3936.5	3897.3	219.5	10.0	10.0	297.6	11.5	170.0	10.0	F2XF2O
-1.68	3731.8	3918.2	3878.4	217.2	10.0	10.0	297.6	11.6	170.0	10.0	F2XF2X
-2.53	5619.8	5899.8	5840.8	217.2	10.0	10.0	299.7	-5.2	170.0	10.0	F2XF2OF2X
-2.53	5638.2	5918.6	5860.1	219.5	10.0	10.0	299.8	-5.4	170.0	10.0	F2XF2OF2O
-2.52	5600.0	5879.7	5820.1	217.2	10.0	10.0	299.7	-5.0	170.0	10.0	F2XF2XF2X
-2.53	5618.5	5898.6	5839.5	219.6	10.0	10.0	299.7	-5.2	170.0	10.0	F2XF2XF2O

3. RADIATION BELT FLUX AND DOSE MODELS

The radiation belts are regions within the earth's magnetosphere where energetic ions and electrons are trapped by the earth's magnetic field at radial distances between 1.1 and 10 earth radii [*Spjeldvik and Rothwell*, 1985]. The energy of these charged particles range between 1 and 200 MeV and are sufficient to penetrate inadequately shielded spacecraft, where they can cause serious damage to electronic components operating on spacecraft, including electronic discharges, degradation, and alteration of memory (single event upsets).

10

The flux and dose models described here are based upon measurements from the Combined Release and Radiation Effects Satellite (CRRES) mission, flown in 1991-1992, and from measurements from various satellites (the NASA models) during the period 1958-1970.

The CRRES models are incorporated in the CRRESRAD, CRRESPRO and CRRESELE software packages. CRRESRAD contains the CRRES dose model, CRRESPRO the proton flux model, and CRRESELE, the electron flux model.

The Combined Release and Radiation Effects Satellite (CRRES) provided the first comprehensive study of the radiation belts since the NASA models. CRRES was launched on 25 July 1990 and provided measurements in a geosynchronous transfer orbit (perigee altitude 350 km, apogee altitude 33000 km, inclination 18°, orbital period 9.85 hr) until 12 October 1991. CRRES contained a wide array of instruments to measure radiation belt fluxes and dosage and their effects on operating components of satellites.

The CRRES models software packages are available from PL in the form of PC executable codes and related binary data files. The programs include an easy-to-use graphics visualization package to facilitate examination of the data by the user and to compute relevant physical properties of the radiation at given locations in space or, where relevant, integrated over satellite orbits. A custom version of the LOKANGL orbital prediction program is provided as part of the CRRES model packages for computation of flux or dose over a specified orbit. The documentation provides a description of the model binary data files that is sufficient to facilitate the use of the models in custom user written applications. The sample output data provided in this section is based upon custom applications written by Radex based upon the binary data model files. Sample output is provided here only for the CRRESRAD model.

The NASA flux models are AP8MAX, AP8MIN (for protons), AE8MAX, and AE8MIN (for electrons) where MAX and MIN refer to solar maximum and solar minimum respectively. Model data files and FORTRAN source code are provided for flux and dosage computations.

3.1 CRRESRAD, The CRRES Dose Model

Radiation dosage is a measure of the energy deposited by radiation in a material per unit mass of the material. It is usually given in rads, where 1 rad = 100 ergs per gram. On CRRES, the dose was measured by the Space Radiation Dosimeter [*Hardy, et al.*, 1985; *Morel, et al.*, 1989], which consisted of 4 silicon detectors shielded by hemispheres of aluminum with thicknesses of 82.5, 232.5, 457.4, and 886.5 mils (1 mil = 1/1000 inch). These correspond to energy thresholds of 20, 35, 50, and 75 MeV for protons, and 1, 2.5, 5, and 10 MeV for electrons. For each detector, dose was accumulated in two channels, LOLET and HILET, corresponding to single event energy depositions of 0.01 - 1 MeV and 1 - 10 MeV, respectively. HILET dose is caused principally by protons of energies 20-100 MeV, and, in major magnetic storms, electrons

11

above 5 MeV. LOLET dose is caused by electrons, bremsstrahlung, and protons above 100 MeV.

A major geomagnetic storm in late March, 1991, so profoundly changed the magnetosphere [*Mullen, et al.*, 1991; *Blake, et al.*, 1992] that two dose models were developed for each shield thickness and dose channel: one for quiet conditions ("Quiet" model), based on data before the storm, and the other for active conditions ("Active" model, based on data after the storm [*Gussenhoven, et al.*, 1992; *Kerns and Gussenhoven*, 1992]. The total number of models available is 36: for each of the 4 thicknesses there are models for each channel (HILET and LOLET) and a model for combined HILET and LOLET. Each of these is given for quiet and active conditions, and the entire CRRES mission. Each model specifies dose rate in bins of L and B/B_0. L is the McIlwain shell parameter [*McIlwain*, 1961] which for a dipole field is the equatorial crossing distance of the magnetic field line through the point of interest. B is the magnetic field intensity at the point of interest, while B_0 is the intensity at the equatorial crossing of the field line. The bin boundaries are defined by:

$$L_i = 0.95 + 0.05 \, I \, R_E, \, 1 <= I <= 141$$

B/B_0 = 1.000, 1.004, 1.020, 1.046, 1.085, 1.140, 1.200, 1.300, 1.400, 1.520, 1.690, 1.880, 2.100, 2.400, 2.730, 3.130, 3.670, 4.350, 5.020, 6.100, 7.410

These models have been incorporated into the CRRESRAD model [*Kerns and Gussenhoven*, 1992], which predicts the radiation dose received in a specified orbit.

The test case shown in Table 8 provides sample dose rates (rads per sec) at the magnetic equator (B/B_0 = 1) for the various channels, conditions, thicknesses and L values indicated. A test on a 40 MHZ Sparc workstation making 10000 calls to the dose model routine required 6.5 seconds. The program which was used to generate Table 8 was written at Radex based upon information about the binary data files provided in the program documentation [*Kerns and Gussenhoven*, 1992].

Table 8. Sample CRRES Dose Model Output

Channel	Condition	Thickness (Mils)	L (RE) 1.50	2.50	4.50
Combined	Combined	82.5	1.834E-02	1.722E-03	1.401E-02
Combined	Combined	232.5	4.048E-03	8.409E-04	1.995E-04
Combined	Combined	457.5	2.171E-03	4.565E-04	2.806E-05
Combined	Combined	886.5	1.199E-03	1.146E-04	1.289E-05
Combined	Quiet	82.5	1.807E-02	4.473E-05	4.849E-03
Combined	Quiet	232.5	4.031E-03	2.676E-05	4.003E-05
Combined	Quiet	457.5	2.150E-03	8.410E-06	1.013E-05
Combined	Quiet	886.5	1.167E-03	4.330E-06	5.810E-06
Combined	Active	82.5	1.869E-02	2.995E-03	2.426E-02
Combined	Active	232.5	4.080E-03	1.469E-03	3.900E-04
Combined	Active	457.5	2.197E-03	7.869E-04	4.779E-05
Combined	Active	886.5	1.233E-03	1.962E-04	2.111E-05
Hilet	Combined	82.5	1.598E-02	4.532E-04	5.060E-06
Hilet	Combined	232.5	3.356E-03	1.913E-04	3.290E-06
Hilet	Combined	457.5	1.538E-03	6.583E-05	0.000E+00
Hilet	Combined	886.5	8.064E-04	1.042E-05	0.000E+00
Hilet	Quiet	82.5	1.582E-02	2.162E-05	0.000E+00
Hilet	Quiet	232.5	3.356E-03	1.071E-05	1.600E-06
Hilet	Quiet	457.5	1.537E-03	3.470E-06	0.000E+00
Hilet	Quiet	886.5	8.003E-04	2.710E-06	0.000E+00
Hilet	Active	82.5	1.619E-02	7.818E-04	6.540E-06
Hilet	Active	232.5	3.369E-03	3.312E-04	5.180E-06
Hilet	Active	457.5	1.542E-03	1.150E-04	0.000E+00
Hilet	Active	886.5	8.131E-04	1.614E-05	4.600E-07
Lolet	Combined	82.5	2.360E-03	1.269E-03	1.401E-02
Lolet	Combined	232.5	6.914E-04	6.497E-04	1.962E-04
Lolet	Combined	457.5	6.326E-04	3.907E-04	2.806E-05
Lolet	Combined	886.5	3.921E-04	1.042E-04	1.289E-05
Lolet	Quiet	82.5	2.246E-03	2.311E-05	4.849E-03
Lolet	Quiet	232.5	6.748E-04	1.605E-05	3.843E-05
Lolet	Quiet	457.5	6.128E-04	4.940E-06	1.013E-05
Lolet	Quiet	886.5	3.664E-04	1.620E-06	5.810E-06
Lolet	Active	82.5	2.499E-03	2.213E-03	2.425E-02
Lolet	Active	232.5	7.108E-04	1.138E-03	3.849E-04
Lolet	Active	457.5	6.555E-04	6.719E-04	4.779E-05
Lolet	Active	886.5	4.197E-04	1.801E-04	2.065E-05

3.2 CRRESPPRO, The CRRES Proton Model

The CRRES proton flux model CRRESPRO [*Meffert and Gussenhoven, 1994*] is based upon measurements made by the Proton Telescope (PROTEL), which was used to measure proton energy and flux on the CRRES satellite in the range 1-100 MeV. PROTEL is a sophisticated proton detector designed to operate in a hostile environment, where it was subjected to a high density flux of electrons, protons and, to a lesser extent, heavier ions, particularly while passing through the radiation (Van Allen) belts. In addition to using passive shielding techniques and magnetic deflection of electrons, it used an array of silicon particle detectors together with an on-board processor, that used coincidence and anti-coincidence in the detector array (detection logic) to reduce false counts. A detailed description of the PROTEL instrument is provided in [*Lynch, et al.*, 1989] and [*Violet, et al., 1992*].

PROTEL consisted of two detector instruments, the low energy head [LEH] (1 - 10 MeV) and the high energy head [HEH] (6 - 100 MeV) and a dedicated processor that processes the raw data from the detectors, and at 1 second intervals, hands off the reduced data to the satellite's telemetry system. The reduced data consist of counts in 24 energy channels (8 for LEH, 16 for HEH) spaced logarithmically in the 1 - 100 MeV energy interval, together with environmental data and raw counts for the solid state particle detectors. Flux data files are provided for 22 energy channels centered at the following proton energies: 1.5, 2.1, 2.5, 2.9, 3.6, 4.3, 5.7, 6.8, 8.5, 9.7, 10.7, 13.2, 16.9, 19.4, 26.3, 30.9, 36.3, 42.3, 47.5, 57.0, 67.5 and 92.9 MeV. For flux/fluence calculations the CRRESPRO model software omits the 3.6 and 16.5 MeV channels because of overlap.

As in the case of the CRRES dose model, two flux models, "Quiet" and "Active", are provided for CRRESPRO, corresponding to data collected before and after the March 1991 storm.

Each model specifies dose rate in bins of L and B/B_0. L is the McIlwain shell parameter [*McIlwain*, 1961] which for a dipole field is the equatorial crossing distance of the magnetic field line through the point of interest. B is the magnetic field intensity at the point of interest, while B_0 is the intensity at the equatorial crossing of the field line. The bin boundaries are defined by:

$$L_i = 0.95 + 0.05 \, i \, R_E, \quad 1 <= i <= 90$$

B/B_0 = 1.000, 1.004, 1.020, 1.046, 1.085, 1.140, 1.200, 1.300, 1.400, 1.520, 1.690, 1.880, 2.100, 2.400, 2.730, 3.130, 3.670, 4.350, 5.020, 6.100, 7.410, 9.088, 11.29, 14.22, 18.16, 23.56, 31.07, 41.47, 57.23, 80.25, 115.4, 170.7, 260.7, 413.4 and 684.6. These values cover approximately $\pm 68°$ magnetic latitude in a dipole field.

14

3.3 CRRESELE, The CRRES Electron Model

The CRRES Electron model CRRESELE [*Brautigam and Bell,* 1995] is based upon measurements made by the High Energy Electron Fluxmeter (HEEF) instrument on the CRRES satellite. HEEF measured the electron flux of 1-10 MeV in ten differential flux number channels. Eight models are provided, six of which correspond to average flux for different levels of solar activity, and two corresponding to observed daily average and daily maximum flux.

The L-bin boundaries are defined by:

$$L_i = 2.45 + 0.05i \ R_E, \ 1 <= i <= 86$$

The B/B_0 bins are the same as in the CRRESPRO model.

3.4 NASA Radiation Belt Trapped Particle Flux Models AP-8 And AE-8

The empirical models AP-8 and AE-8 describe radiation belt trapped proton and electron fluxes, respectively, in the ion energy range 0.1-400 MeV and electron energy range 0.04-7 MeV. They are based on data from 1958 to 1970. They are described briefly by *Jordan* [1989] with further details given in the references therein. The models give integral or differential omnidirectional flux as a functions of L [*McIlwain,* 1961] and B/B_0, where B is the magnetic field magnitude at the point of interest, and B_0 is the equatorial B value, given by:

$$B_0 (gauss) = 0.311653/L^3$$

For each model there is a solar maximum (AP8MAX, AE8MAX) and solar minimum (AP8MIN, AE8MIN) version. Other variations found in the data, including those related to magnetic storms and local time, are averaged in these models. The data supporting the earliest models was contaminated by the Starfish nuclear detonation (9 July 1962), but this has been removed in the present models.

Table 1 of *Sawyer and Vette* [1976] lists the data sources for AP-8. These authors found that in the inner zone (L < 2.5 R_E) the fluxes were generally stable except for responses to major storms, the decay of the starfish population, and solar cycle dependence at altitudes less than 1000 km. In the outer zone, nonadiabatic storm-related flux changes were observed, with recovery time constants ranging from months to years. Modeling of the storm-related variations was not attempted because of the difficulty in generalizing the details of specific storms. The model solar cycle variation was derived from the satellite Azur data. Although earlier models were generated by analytic fits to power law or exponential spectra, the present AP-8 models are purely tabular in form, because of the difficultly in fitting the entire 0.1-400 MeV range to such simple forms.

The AE-8 models were derived from a combination of the AE-4, AE-5 and AE-6 models with new data from satellites OV1-3, OV1-19, AZUR, and ATS-6. The AE-4 model was derived from the measurements of 23 instruments flown on 11 satellites from 1959 to 1968. The AE-5 model was derived from data between December, 1964, and December, 1967, covering the inner zone only ($L = 1.2 - 2.8\,R_E$). The form used for AE-8, called AE-5 1975 projected, models solar minimum conditions. AE-6 is used to model solar maximum. Both AE-5 1975 projected and AE-6 have had the Starfish contribution removed. Unlike earlier models, which were tabulated separately for inner and outer zones, the AE-8 model tables are combined, just like the AP-8 models. The AP-8 and AE-8 tables use common format, permitting them to be used in the same software.

The sample output in Table 9 was generated for 1 MeV ions (AP8MAX) and electrons (AE8MAX) for solar maximum conditions.

A test on a 40 MHz Sparc IPX workstation making 10000 calls, each reading in a model table from a data file, required 340 sec. A second test, also making 10000 calls, but reading in a table only on the first call, required 0.4 sec.

Table 9. Sample NASA Model Output (1 MeV Particles)

AP8MAX MODEL

L	B/B0 1.0	2.0	4.0	6.0	8.0	10.0	30.0
1.0	0.000E+00	0.000E+00	0.000E+00	0.000E+00	0.000E+00	0.000E+00	0.000E+00
2.0	6.928E+00	5.904E+00	4.935E+00	3.333E+00	0.000E+00	0.000E+00	0.000E+00
3.0	7.580E+00	6.764E+00	6.203E+00	5.884E+00	5.646E+00	5.444E+00	0.000E+00
4.0	6.493E+00	5.835E+00	5.390E+00	5.159E+00	4.985E+00	4.870E+00	4.171E+00
5.0	4.527E+00	3.599E+00	3.080E+00	2.848E+00	2.683E+00	2.541E+00	1.977E+00
6.0	3.415E+00	2.491E+00	2.024E+00	1.811E+00	1.649E+00	1.543E+00	9.740E-01
7.0	2.669E+00	1.826E+00	1.369E+00	1.174E+00	1.043E+00	9.305E-01	3.999E-01
8.0	1.779E+00	1.102E+00	8.134E-01	6.763E-01	5.796E-01	5.118E-01	1.023E-01
9.0	8.897E-01	4.562E-01	3.102E-01	2.390E-01	1.897E-01	1.458E-01	0.000E+00
10.0	0.000E+00	0.000E+00	0.000E+00	0.000E+00	0.000E+00	0.000E+00	0.000E+00

AE8MAX MODEL

L	B/B0 1.0	2.0	4.0	6.0	8.0	10.0	30.0
1.0	0.000E+00	0.000E+00	0.000E+00	0.000E+00	0.000E+00	0.000E+00	0.000E+00
2.0	4.893E+00	4.234E+00	3.390E+00	2.487E+00	0.000E+00	0.000E+00	0.000E+00
3.0	6.033E+00	5.877E+00	5.471E+00	5.192E+00	4.983E+00	4.816E+00	3.567E+00
4.0	6.505E+00	6.405E+00	6.221E+00	6.086E+00	5.979E+00	5.913E+00	5.470E+00
5.0	6.446E+00	6.350E+00	6.171E+00	6.042E+00	5.932E+00	5.877E+00	5.507E+00
6.0	5.999E+00	5.903E+00	5.724E+00	5.599E+00	5.489E+00	5.438E+00	5.101E+00
7.0	5.414E+00	5.318E+00	5.140E+00	5.018E+00	4.907E+00	4.858E+00	4.536E+00
8.0	4.462E+00	4.366E+00	4.187E+00	4.066E+00	3.955E+00	3.907E+00	3.593E+00
9.0	2.875E+00	2.782E+00	2.609E+00	2.505E+00	2.401E+00	2.345E+00	2.056E+00
10.0	6.982E-01	6.288E-01	4.899E-01	4.125E-01	3.615E-01	3.105E-01	3.228E-02

4. MODELS OF AURORAL PRECIPITATION

The morphology and fluxes of precipitating electrons and ions in the Earth's auroral region is an important input to many theoretical calculations and is critical to the planning of auroral imaging missions. For many years, the DMSP satellites have been collecting data on the flux of energetic electrons and ions over the poles. These data have been accumulated and binned as a function of geomagnetic coordinates and geophysical parameters. To facilitate the use of these binned averages in other programs, the averages have been fit to functional forms. These models result in compact and efficient subroutines by which fluxes and related properties can be evaluated.

There are two distinct auroral models available. Both give electron and ion number and energy flux as a function of corrected geomagnetic latitude (λ) and magnetic local time (MLT). They differ in that one set of models assumes that the variation in flux at a specific location is due to variation in the value of K_p. The other set assumes that the variation can be described by the simultaneous specification of the solar wind velocity and the interplanetary magnetic field component B_z. These will be described separately although their use and output is basically the same.

4.1 Models Driven by K_p

The K_p driven models consist of two routines, one for electrons and another for ions. A complete description for both the data processing and modeling for the electrons can be found in *Hardy, et al.* [1987]. The data processing used for the ion model generation is described by *Hardy, et al.* [1989] and the model generation is described in *Hardy, et al.* [1991]. However, each of the auroral region "maps" for a specific value of K_p is treated independently. The latitudinal dependence of the base 10 logarithm of the flux at each discrete MLT is examined and fit to an Epstein transition function. The first order Epstein function, which was used for the electrons, is given by

$$e(\lambda) = r + S_1(\lambda - \lambda_0) + (S_2 - S_1) \ln \frac{1 - S_1/(S_2 e^{-(\lambda - \lambda_0)})}{1 - S_1/S_2}$$

This complicated expression has a comparatively simple behavior, since e is equal to r at λ_0 and the curve is linear with slope S_1 and S_2 for $\lambda \ll \lambda_0$ and $\lambda \gg \lambda_0$ respectively. The first order function is used for electron number and energy flux and for Hall and Pederson conductivity. A second order function is used for the ion number and energy flux because the curves were somewhat broader than the electron parameters as a function of latitude. The second order Epstein function allows two points to be set, namely the values of the functions at λ_0 and λ_1.

The coefficients of the Epstein functions were then expanded in a Fourier series for each map to further reduce the size requirements of the model and to provide another degree of smoothing. Each K_p map in the model is considered separately and so interpolation in this dimension is not available.

17

Two FORTRAN subroutines, 'elemod.f' and 'ionmod.f', are available to evaluate the coefficients of the model. These require the data files ELECOEF.DAT and IONCOEF.DAT. Evaluation of a full map between the valid latitudes of 50° and 90° at 1° increments requires about 8 seconds with ASCII output and about 4 seconds without output on a Sparc 10 workstation. Table 10 below shows sample output for ions and electron fluxes and conductivities. The results of the model generation are shown in Table 10 for both the noon and midnight slice at a K_p of 2.

Table 10. Sample Output from Auroral K_p Models for K_p of 2

	Midnight Sector						Noon Sector					
λ	Σ_H	Σ_P	J_E^-	J_N^-	J_E^+	J_N^+	Σ_H	Σ_P	J_E^-	J_N^-	J_E^+	J_N^+
50.0	0.00	0.00	1.000E+06	1.000E+06	1.000E+04	1.000E+04	0.00	0.00	1.000E+06	1.000E+06	1.000E+04	1.000E+04
52.0	0.00	0.00	1.000E+06	1.000E+06	1.000E+04	1.000E+04	0.00	0.00	1.000E+06	1.000E+06	1.000E+04	1.000E+04
54.0	0.00	0.00	1.000E+06	1.000E+06	1.000E+04	1.000E+04	0.00	0.00	1.000E+06	1.000E+06	1.000E+04	1.000E+04
56.0	0.00	0.00	1.000E+06	1.087E+06	1.000E+04	1.000E+04	0.00	0.00	1.000E+06	1.000E+06	1.000E+04	1.000E+04
58.0	0.00	0.00	2.112E+06	2.982E+06	1.000E+04	1.000E+04	0.00	0.00	1.000E+06	1.000E+06	1.000E+04	1.000E+04
60.0	0.00	0.00	1.022E+07	8.177E+06	1.000E+04	1.163E+04	0.00	0.00	1.000E+06	1.000E+06	1.000E+04	1.000E+04
62.0	4.77	2.44	4.812E+07	2.233E+07	2.248E+06	2.898E+05	0.00	0.00	1.312E+06	1.000E+06	1.000E+04	1.000E+04
64.0	9.62	5.40	1.902E+08	5.925E+07	5.017E+07	2.450E+06	0.00	0.00	3.505E+06	1.000E+06	1.000E+04	1.506E+04
66.0	9.93	6.44	3.767E+08	1.320E+08	5.981E+07	4.602E+06	1.42	0.41	9.338E+06	1.000E+06	8.165E+04	3.753E+04
68.0	7.94	5.78	3.066E+08	1.716E+08	3.412E+07	3.166E+06	3.39	1.14	2.437E+07	3.020E+06	1.070E+06	9.366E+04
70.0	5.49	4.67	1.795E+08	1.360E+08	1.630E+07	1.636E+06	5.10	1.84	5.593E+07	9.583E+06	2.928E+06	2.354E+05
72.0	2.98	3.48	9.928E+07	9.368E+07	7.186E+06	8.074E+05	5.61	2.32	8.172E+07	3.028E+07	5.337E+06	6.192E+05
74.0	0.55	2.28	5.446E+07	6.308E+07	3.100E+06	3.959E+05	4.26	2.14	7.312E+07	9.264E+07	9.026E+06	1.893E+06
76.0	0.55	1.07	2.984E+07	4.235E+07	1.333E+06	1.939E+05	2.09	1.34	5.585E+07	2.326E+08	1.392E+07	6.060E+06
78.0	0.55	0.55	1.635E+07	2.842E+07	5.731E+05	9.498E+04	0.55	0.55	4.156E+07	3.022E+08	1.459E+07	1.059E+07
80.0	0.55	0.55	1.000E+07	1.907E+07	2.463E+05	4.652E+04	0.55	0.55	3.081E+07	2.018E+08	8.070E+06	6.113E+06
82.0	0.55	0.55	1.000E+07	1.280E+07	1.059E+05	2.279E+04	0.55	0.55	2.283E+07	1.099E+08	3.316E+06	2.100E+06
84.0	0.55	0.55	1.000E+07	1.000E+07	4.550E+04	1.116E+04	0.55	0.55	1.692E+07	5.794E+07	1.287E+06	6.528E+05
86.0	0.55	0.55	1.000E+07	1.000E+07	1.956E+04	1.000E+04	0.55	0.55	1.254E+07	3.040E+07	4.956E+05	2.001E+05
88.0	0.55	0.55	1.000E+07	1.000E+07	1.000E+04	1.000E+04	0.55	0.55	1.000E+07	1.594E+07	1.906E+05	6.120E+04
90.0	0.55	0.55	1.000E+07	1.000E+07	1.000E+04	1.000E+04	0.55	0.55	1.000E+07	1.000E+07	7.330E+04	1.871E+04

4.2 Models Driven by IMF and Solar Wind

Auroral precipitation models in the other set are driven by the values of the Interplanetary Magnetic Field (IMF) B_z and the Solar Wind Speed (SWS). Documentation for the generation of these models can be found in *Brautigam, et al.* [1991]. They differ also in that there is a separate set of data files and routines for the conductivity. The fitting was done with the same functional forms except that second order Epstein functions were used for the electron fluxes because they were somewhat broader than in the K_p versions. Some rough comparisons of these two models with SSJ4 fluxes pass-by-pass indicate that they are roughly equivalent in accuracy, however, it is ultimately the user's responsibility to determine which set of models best serves the purpose. This is to say that neither the K_p or the IMF/SWS model is recommended over the other. The correspondence between map number and IMF/SWS conditions is given in Table 11.

18

Table 11. Map Numbers Corresponding to Various IMF/SWS Conditions

B_z \ SWS	346 km/s	408 km/s	485 km/s	572 km/s	677 km/s
-4.5 nT	map 1	map 7	map 13	map 19	map 25
-2.2 nT	map 2	map 8	map 14	map 20	map 26
-0.7 nT	map 3	map 9	map 15	map 21	map 27
+0.7 nT	map 4	map 10	map 16	map 22	map 28
+2.2 nT	map 5	map 11	map 17	map 23	map 29
+4.5 nT	map 6	map 12	map 18	map 24	map 30

As before, the models are in the form of subroutines called *ionimf.f*, *eleimf.f*, and *conimf.f* and require the data files IONIMF.DAT, ELEIMF.DAT, and CONIMF.DAT respectively. Time requirements for the IMF/SWS models are about the same as for the K_p versions. Table 12 below gives the expected output from map 15.

Table 12. Sample output from Auroral IMF/SWS Models for Map 15

			Midnight Sector							Noon Sector		
λ	Σ_H	Σ_P	J_E^-	J_N^-	J_E^+	J_N^+	Σ_H	Σ_P	J_E^-	J_N^-	J_E^+	J_N^+
50.0	0.50	0.25	3.732E+01	1.906E+02	1.000E+00	1.000E+00	0.50	0.25	3.286E+01	3.047E+01	1.000E+00	2.074E+02
52.0	0.50	0.25	4.199E+02	1.447E+03	1.000E+00	1.000E+00	0.50	0.25	1.701E+02	1.004E+02	1.000E+00	4.404E+02
54.0	0.50	0.25	4.725E+03	1.098E+04	8.895E+00	6.130E+00	0.50	0.25	8.810E+02	3.307E+02	1.000E+00	9.351E+02
56.0	0.50	0.25	5.315E+04	8.332E+04	2.911E+02	1.314E+02	0.50	0.25	4.562E+03	1.089E+03	1.000E+00	1.985E+03
58.0	0.50	0.25	5.968E+05	6.309E+05	9.434E+03	2.788E+03	0.50	0.25	2.362E+04	3.588E+03	1.000E+00	4.215E+03
60.0	0.50	0.25	6.611E+06	4.708E+06	2.852E+05	5.464E+04	0.50	0.25	1.223E+05	1.182E+04	6.730E+00	8.949E+03
62.0	3.54	2.97	6.660E+07	3.178E+07	5.794E+06	6.830E+05	0.50	0.25	6.323E+05	3.893E+04	1.594E+02	1.900E+04
64.0	10.55	6.89	4.013E+08	1.324E+08	3.893E+07	2.574E+06	1.83	0.25	3.238E+06	1.283E+05	3.723E+03	4.034E+04
66.0	16.01	9.36	7.314E+08	2.281E+08	7.301E+07	3.633E+06	3.85	0.72	1.549E+07	4.227E+05	7.913E+04	8.565E+04
68.0	16.69	9.16	6.103E+08	2.509E+08	4.887E+07	3.003E+06	5.74	1.20	5.213E+07	1.399E+06	1.014E+06	1.820E+05
70.0	12.99	7.58	4.250E+08	2.511E+08	2.204E+07	1.666E+06	6.94	1.67	8.298E+07	4.754E+06	4.120E+06	3.886E+05
72.0	8.04	5.73	2.839E+08	2.387E+08	9.247E+06	8.109E+05	6.29	2.09	8.468E+07	1.849E+07	8.034E+06	8.568E+05
74.0	2.90	3.83	1.708E+08	1.795E+08	3.841E+06	3.863E+05	4.24	2.23	7.783E+07	8.814E+07	1.280E+07	2.127E+06
76.0	0.50	1.93	6.455E+07	6.499E+07	1.593E+06	1.834E+05	1.82	1.83	6.652E+07	2.688E+08	1.582E+07	5.306E+06
78.0	0.50	0.25	1.124E+07	1.188E+07	6.606E+05	8.708E+04	0.50	1.13	4.254E+07	2.122E+08	9.596E+06	6.171E+06
80.0	0.50	0.25	5.816E+06	7.644E+06	2.740E+05	5.438E+04	0.50	0.38	1.577E+07	7.235E+07	3.045E+06	2.174E+06
82.0	0.50	0.25	5.816E+06	7.644E+06	2.326E+05	5.438E+04	0.50	0.25	5.816E+06	2.051E+07	8.034E+05	4.701E+05
84.0	0.50	0.25	5.816E+06	7.644E+06	2.326E+05	5.438E+04	0.50	0.25	5.816E+06	7.644E+06	2.326E+05	9.311E+04
86.0	0.50	0.25	5.816E+06	7.644E+06	2.326E+05	5.438E+04	0.50	0.25	5.816E+06	7.644E+06	2.326E+05	5.438E+04
88.0	0.50	0.25	5.816E+06	7.644E+06	2.326E+05	5.438E+04	0.50	0.25	5.816E+06	7.644E+06	2.326E+05	5.438E+04
90.0	0.50	0.25	5.816E+06	7.644E+06	2.326E+05	5.438E+04	0.50	0.25	5.816E+06	7.644E+06	2.326E+05	5.438E+04

5. MAGNETIC FIELD MODELS; CORRECTED GEOMAGNETIC COORDINATES

The Earth's magnetic field is usually modeled as the sum of the "main" internal magnetic field, which is, for the most part, attributed to currents within the earth's core, and an "external" field, attributed to ionospheric and magnetospheric currents. For the "main" field the standard reference models are the IGRF/DGRF models, described below. The Hilmer-Voight, Tsyganenko-Usmanov, and Olson-Pfitzer external models are also described below.

Corrected Geomagnetic (CGM) Coordinates are based upon internal magnetic field models, and provide a convenient tool for the analysis of data of charged particles (electron, protons and other ions) moving in the ionosphere and in the radiation belts. FORTRAN routines that convert geographic coordinates to CGM and the inverse are also described below. CGLALO and CGLALO_INV provide table interpolation for conversion for low altitudes, and SFC_CONVERT_GEO_COORD provide altitude dependent conversion for altitudes 0-7200 km. A description of these routines is provided below.

5.1 IGRF/DGRF Internal Magnetic Field Models

The International Geomagnetic Field Reference Field models represent the "main" internal magnetic field. Since the internal magnetic field changes with time, the model is updated once every 5 years by the International Association of Geomagnetism and Aeronomy (IAGA) [*Barton*, 1996; *Langel*, 1991; *Langel, et al.*, 1988]. Mathematically the model is represented as the negative gradient of a scalar potential V represented as a sum of spherical harmonics to degree and order 10:

$$V = a \sum_{n=1}^{10} \left(\frac{a}{r} \right)^{n+1} \sum_{m=0}^{n} (g_n^m \cos m\phi + h_n^m \sin m\phi) \, P_n^m(\sin \theta) \qquad (3)$$

where a is the mean earth radius, 6371.2 km, and (r, θ, ϕ) are the spherical coordinates of the position. To convert from geodetic to spherical coordinates, IAGA recommends use of the International Astronomical Union (IAU) reference ellipsoid, with equatorial radius 6378.16 km and flattening ratio 1/298.25.

The models have been derived from data provided by observatories, ships, aircraft, and satellites. Daily and annual averages of the measurements are used in least squares fits to compute the spherical harmonic coefficients. If possible, daily values used for computing the fits are limited to magnetically quiet days, to avoid perturbations by external currents. This problem is particularly troublesome for satellite data. Many satellites pass through regions of external currents, for which the spherical harmonic representation is not valid (curl of B is not zero). Principally there exist field-aligned currents, running parallel to field lines between the magnetosphere and the high-latitude ionosphere.

The field aligned currents perturb mainly the direction, but not the magnitude of the field. Therefore only the magnitude is used in the analysis. *Langel and Estes* [1985] found that eastward flowing auroral electrojets underneath satellite MAGSAT produced asymmetries in local time, with significant differences between dawn and dusk measurements. Data for the subsequent analysis were therefore carefully selected, giving precedence to dawn, where the effect was minimal. Where necessary, data from dusk were used with latitude-dependent corrections.

The existing models consists of a series of DGRF (Definitive Geomagnetic Reference Field) models at 5-year intervals from 1945 through 1990, and an IGRF model for 1995, where the latter includes coefficients for the predicted secular variation for the years 1995 thru 2000. Each DGRF model is specified by a set of coefficients g_n^m, h_n^m. Values of the coefficients between successive DGRF epochs are obtained by linear interpolation. The IGRF models include the latter and estimates of their first time derviatives. The DGRF models are expected not to change, since no new data is likely to be available for them. For the period between 1990 and 1995 interpolation is performed between DGRF90 and the set of coefficients g_n^m, h_n^m from IGRF95.

In the year 2000, the IGRF95 model will be replaced by a DGRF95 model based on new observational data, and a new predictive model IGRF 2000 will become available, with an estimated secular variation for the following 5 years.

To take into account the effects of the external fields, it is customary to augment the DGRF and IGRF models with external field models, some of which are described below. The IGRF models also form the basis of computations of Corrected Geomagnetic Coordinate routines such as CGLALO and SFC_CONVERT_GEO_COORD.

Several codes are available to compute both the magnetic field and derived properties, such as L-shell. We use here the NASA package, which employs the inverse coordinate method of *Kluge* [1972]. Table 13 presents a sample output for 1 Jan, 0 hr UT, in the indicated years. The total magnetic field, and its northward, eastward and downward components are given in Gauss. The L-computation routine returns a code (ICODE) which is 1 to indicate successful computation by the normal method of numerical integration, 2 to indicate failure because the conjugate point is below the earth's surface (the value output is meaningless), and 3 to indicate that L was computed by an approximate method, applicable at very large L.

On a 40 MHZ Sparc IPX workstation, the average times, per 10000 calls, for the various computations are:

Model coefficients	102 sec
Magnetic field vector	0.7 sec
L	7.5 sec

Table 13. Sample IGRF90 Model Output

YEAR	ALTITUDE	LAT	LON	B(NORTH)	B (EAST)	B (DOWN)	B(TOTAL)	L	ICODE
1946	800	40	0	0.168976	-0.027447	0.254116	0.306400	1.7909	1
1956	800	40	0	0.171061	-0.024426	0.254050	0.307246	1.7773	1
1966	800	40	0	0.173115	-0.021878	0.253273	0.307563	1.7608	1
1976	800	40	0	0.175535	-0.019309	0.252736	0.308320	1.7381	1
1986	800	40	0	0.177165	-0.015420	0.251816	0.308280	1.7198	2
1996	800	40	0	0.178122	-0.012116	0.251588	0.308498	1.7068	2
2006	0	40	0	0.253320	-0.010634	0.363182	0.442928	1.4601	2
2006	5000	40	0	0.042920	-0.005833	0.063948	0.077237	2.9277	1
2006	10000	40	0	0.013862	-0.002348	0.022052	0.026153	4.3749	1
2006	15000	40	0	0.006101	-0.001142	0.010101	0.011856	5.8417	1
2006	20000	40	0	0.003205	-0.000635	0.005443	0.006348	7.3239	1
2006	25000	40	0	0.001887	-0.000388	0.003262	0.003788	8.7915	1
2006	800	15	0	0.221757	-0.019374	0.046358	0.227378	1.1294	1
2006	800	25	0	0.216404	-0.015066	0.137736	0.256961	1.2289	1
2006	800	35	0	0.193437	-0.012634	0.217962	0.291694	1.4844	1
2006	800	45	0	0.161603	-0.011998	0.280723	0.324137	2.0204	2
2006	800	55	0	0.127604	-0.012523	0.326832	0.351082	3.0926	2
2006	800	65	0	0.094509	-0.013060	0.360054	0.372480	5.6217	1
2006	800	40	50	0.182531	0.010100	0.281426	0.335590	1.6364	1
2006	800	40	100	0.196909	-0.003280	0.311539	0.368566	1.5330	1
2006	800	40	150	0.193310	-0.010558	0.255774	0.320781	1.5213	1
2006	800	40	200	0.166680	0.037719	0.260741	0.311754	1.7902	1
2006	800	40	250	0.145364	0.029618	0.337651	0.368804	2.4993	1
2006	800	40	300	0.142618	-0.042709	0.318770	0.351822	2.6275	1

5.2 Hilmer-Voigt Magnetospheric Magnetic Field Model

Unlike the internal field, there is no standard reference model for the external field. Several models have been developed with varying degrees of sophistication. Among the most elegant is the Hilmer-Voigt model [*Hilmer and Voigt*, 1995; *Hilmer*, 1989]. This model seeks to provide realistic, yet mathematically tractable, representations of known essential features of the magnetosphere. The condition $\nabla \cdot \mathbf{B} \approx 0$ is satisfied throughout. Contributions due to magnetopause currents, ring currents, and cross-tail currents are included. The magnetopause field in the Hilmer-Voigt model "shields" the dominant dipole portion of the internal field from the solar wind by canceling the dipole field's normal component along the magnetopause [*Voigt*, 1981]. The magnetopause consist of a hemisphere facing the sun with a cylinder of equal radius extending anti-sunward. The ring currents consist of eastward and westward flowing currents, cylindrically symmetric with respect to the earth. They have a simple mathematical form, first used by *Tsyganenko and Usmanov* [1982], whose model, however, has only a westward flowing current. The eastward current, at distances less than 3-4 R_E, is inferred from observations of a maximum in the plasma pressure, which in equilibrium satisfies the condition $\mathbf{J} \times \mathbf{B} = \nabla P$. The maximum in P forces ∇P to change sign, which means that the current density must change sign. The cross-tail currents, embedded in the night-side plasma sheet, are represented by current filaments, flowing infinitely from dawn to dusk, in a series of 16 plane segments. The segments

22

are positioned and oriented to simulate a sheet with a specified near-earth edge which is in the earth's magnetic equator. When the earth's dipole is not tilted with respect to the earth-sun line, the entire sheet remains on the equator. When the dipole is tilted, the sheet curves toward an orientation which, at large distances from the earth, is parallel to the GSM equator (the plane through the earth-sun line that is normal to the plane containing the sun and the dipole).

The model is driven by four parameters: dipole tilt, magnetospheric standoff distance (noon equatorial intersection of the magnetopause), geomagnetic activity index D_{st}, and the noon equatorward boundary of the diffuse aurora. The standoff distance and dipole tilt determine the magnetopause field. The ring and cross-tail currents are described by structural and strength parameters which are determined by a procedure that forces the model field to reproduce D_{st} and known ΔB patterns in the noon-midnight meridian, while also satisfying the requirement that the cross-tail inner edge maps to the equatorward boundary of diffuse aurora. In practice the strength and structural parameters are prestored on file for specific configurations. At run time the configuration closest to the specified set of inputs (tilt, standoff, D_{st}, and equatorward boundary) is chosen.

An option exists to simulate substorm diversion of the cross-tail currents near the noon-midnight meridian, by adding an eastward current to the normal westward current. One strength parameter and two structure parameters are determined to reproduce a specific midnight geosynchronous recovery of B_z and to maintain positive B_z over the entire equator.

The sample output shown in Table 14 was generated at 8 locations, for two configurations defined by the parameters shown: standoff distance, tilt, D_{st}, and equatorward edge (EQEDGE). The 8 locations are specified in the GSM coordinate system. On a 40MHz Sparc workstation, the Hilmer-Voigt model takes 0.3 seconds for initialization, which must take place whenever any of the model input parameters changes. The inititialization includes setting up the structural and strength parameters, based on the set of input parameters, and performance of numerical tasks which depend on these parameters. Initialization + 10000 calls to compute point model magnetic field vectors requires 3.2 sec.

Table 14. Sample Hilmer-Voigt Output

```
Standoff = 10.00 RE    Tilt =  10.00 Deg   DST =  -20.0 nT    EQEDGE =   68.0 Deg

   X (RE)     Y (RE)     Z (RE)      BX (nT)    BY (nT)    BZ (nT)    BTOT (nT)
     2.         0.         0.        -1334.7      0.0       3765.0      3994.6
     0.         2.         0.          664.9     -0.3       3761.8      3820.1
     0.         0.         2.          668.2      0.0      -7584.7      7614.1
     6.         0.         0.          -47.9      0.0        143.5       151.3
     0.         6.         0.           24.5     -0.8        132.5       134.7
     0.         0.         6.           33.6      0.0       -302.6       304.5
    -2.         0.         0.        -1336.4      0.0       3758.4      3988.9
    -6.         0.         0.          -54.0      0.0        121.3       132.8

Standoff =  7.00 RE    Tilt =  10.00 Deg   DST = -200.0 nT    EQEDGE =   55.0 Deg

   X (RE)     Y (RE)     Z (RE)      BX (nT)    BY (nT)    BZ (nT)    BTOT (nT)
     2.         0.         0.        -1362.9      0.0       3661.8      3907.2
     0.         2.         0.          645.7     -2.1       3638.7      3695.5
     0.         0.         2.          663.8      0.0      -7796.6      7824.8
     6.         0.         0.          -11.2      0.0        301.6       301.8
     0.         6.         0.           30.8     -4.6        165.8       168.7
     0.         0.         6.           71.1      0.0       -332.9       340.4
    -2.         0.         0.        -1374.7      0.0       3622.4      3874.5
    -6.         0.         0.          -71.8      0.0        144.8       161.6
```

5.3 Olson-Pfitzer Quiet Tilt-Dependent External Field Model

The Olson-Pfitzer tilt dependent external field model [*Olson and Pfitzer*, 1977] includes the field contributions from the magnetopause, tail, and ring currents. These contributions are formed and oriented by the solar wind, and are thus tilted as a function of season and time, independent of Earth-dipole axis coordinates. Tilt is defined as the complement of the Sun-dipole angle. The total external field is obtained by vectorially adding this component to the internal field, which is defined by a standard model such as IGRF 1985 [*Barraclough*, 1987]. The Olson-Pfitzer model revises an earlier tilt-averaged model that did not adequately represent the zero tilt case, particularly at large distances on the midnight equator.

This model is valid for all tilts of the earth's dipole. There is no dependence on magnetic activity - the model is an average for quiet conditions (K_p = 0, 1). The code has been optimized for the near earth region, and is valid to 15 R_E. Beyond that, the field diverges rapidly, and a template sets the field to zero. To improve computational speed, the external field is set to zero below 2 R_E, since the external field contribution to the total field is negligible in this region.

Magnetopause currents and their resulting contributions to the field are computed numerically; ring and cross-tail currents are constructed from a conceptual system of wires. Parameters specifying the wires (position, orientation, size, and shape), their currents, and the magnetopause shape are adjusted so that the resulting total external field fits observations from the inner magnetosphere and the tail. The resulting field is then fit by linear least squares to an analytic series [*Bass and Jordan*, 1990].

24

The sample runs summarized in Table 15 were generated using code incorporating the IGRF 1985 internal field model. These examples show the model's seasonal variation, as well as the variation with hour (UT), radius (in km), and latitude. Program output consists of the components of the model magnetic field in geocentric coordinates, along with the total field (in nanoTesla). The time required for the external field calculation is small: 10,000 total field calculations require 57 seconds on a 40 MHz Sparc IPX workstation, while 51 seconds are needed to compute only the internal field.

Table 15. Olson-Pfitzer Tilt Dependent External Field Model Sample Runs

Year	Day	UT	Radius	Lat	Lon	B_x	B_y	B_z	B_{tot}
1994	1	0	50000	40	0	-112.153	-8.327	-40.400	119.50
1994	50	0	50000	40	0	-116.544	-9.165	-38.527	123.09
1994	100	0	50000	40	0	-122.376	-8.504	-35.006	127.57
1994	150	0	50000	40	0	-126.346	-8.007	-31.660	130.50
1994	200	0	50000	40	0	-126.256	-8.738	-31.913	130.52
1994	250	0	50000	40	0	-121.850	-8.262	-35.283	127.12
1994	300	0	50000	40	0	-115.761	-7.586	-38.585	122.26
1994	100	0	50000	40	0	-122.376	-8.504	-35.006	127.57
1994	100	4	50000	40	0	-111.975	4.698	-24.178	114.65
1994	100	8	50000	40	0	-95.599	0.748	-7.170	95.87
1994	100	12	50000	40	0	-90.374	-15.514	3.603	91.77
1994	100	16	50000	40	0	-97.813	-30.260	-9.118	102.79
1994	100	20	50000	40	0	-116.311	-26.549	-31.476	123.39
1994	100	24	50000	40	0	-122.480	-8.482	-34.927	127.64
1994	100	0	20000	40	0	-1429.696	-128.736	-256.545	1458.22
1994	100	0	30000	40	0	-444.255	-38.485	-106.030	458.35
1994	100	0	40000	40	0	-207.373	-16.408	-56.742	215.62
1994	100	0	50000	40	0	-122.376	-8.504	-35.006	127.57
1994	100	0	60000	40	0	-84.982	-4.962	-23.412	88.29
1994	100	0	70000	40	0	-66.576	-3.885	-14.995	68.35
1994	100	0	80000	40	0	-55.129	-4.767	-6.257	55.69
1994	100	0	50000	-80	0	62.894	-12.968	-122.470	138.28
1994	100	0	50000	-60	0	106.151	-10.897	-89.105	139.02
1994	100	0	50000	-40	0	108.226	-9.605	-30.936	112.97
1994	100	0	50000	-20	0	64.434	-8.843	25.109	69.72
1994	100	0	50000	0	0	-10.325	-8.356	47.366	49.19
1994	100	0	50000	20	0	-83.513	-8.179	21.993	86.75
1994	100	0	50000	40	0	-122.376	-8.504	-35.006	127.57
1994	100	0	50000	60	0	-112.236	-9.804	-91.097	144.88
1994	100	0	50000	80	0	-59.826	-12.180	-119.158	133.89

5.4 Tsyganenko-Usmanov External Field Model

The Tsyganenko-Usmanov external field model [*Tsyganenko and Usmanov*, 1982] is expressed as the sum of contributions from ring currents, cross-tail currents, and magnetopause currents. No attempt was made to provide an accurate model of the near-Earth region, due to limited data coverage, but this model provides reasonable results from 5 R_E to 20 R_E. This model is the forerunner of the Tsyganenko model [*Tsyganenko*, 1987].

The ring and tail contributions are expressed analytically by functions that are curls of vector potentials; therefore, their divergences vanish identically. The model employs a mathematically simple azimuthally symmetric ring current circulating around the dipole. The ring current flow direction is westward, independent of distance from the earth. The tail current is represented as flowing mainly from dawn to dusk on a flat "sheet". The contribution of the magnetopause current is represented by tilt-dependent products of polynomials and decaying exponentials [*Bass and Jordan*, 1990].

The database for the Tsyganenko-Usmanov model consists of data from the Mead-Fairfield model, and data from HEOS-1 and HEOS-2. The Mead-Fairfield data base consists of averaged measurements from magnetometers on board Explorer 33, Explorer 34, Explorer 41, and Explorer 43. These data were averaged over half-Earth radii - typically 10 to 15 minutes. The Tsyganenko-Usmanov data set has a gap in the near-Earth region, making it unreliable inside of 5 R_E. There is also minimal data coverage beyond 20 R_E, defining the model's practical limit.

5.5 Corrected Geomagnetic Coordinate Codes: CGLALO, GGLALO_INVERSE, SFC_CONVERT_GEO_COORD

Ionospheric processes and the motion of charged particles, both in the ionosphere and the radiation belts, are determined by Earth's magnetic field. In the early period of space exploration, the use of Geomagnetic Coordinates, a spherical coordinate system aligned with an earth centered dipole, was suitable for the analysis of rocket and satellite based observations of the motion of charged particles and ionospheric phenomena. As improvements in observational techniques were developed, and more precise measurements became possible, it became necessary to develop coordinates that more closely reflected the actual magnetic field of the Earth. These Corrected Geomagnetic Coordinates (CGM) systems were based upon magnetic field line tracing using magnetic field models, in which the magnetic field is represented as the negative gradient of a magnetic scalar potential.

The original procedure to compute CGM coordinates was as follows: A real field line from the Earth's surface is traced to the equator of the centered dipole. This point is defined to be the equivalent to a line trace along a centered dipole field. The latitude and longitude of the landing point in centered dipole coordinates are the desired "corrected" geomagnetic coordinates.

CGM coordinates, unlike geographic coordinates or centered dipole magnetic coordinates, are distorted, the distortion being a reflection of the deviation of the Earth's magnetic field from a centered dipole field. An Earth globe based upon CGM coordinates will distort distances and angles between pairs of points compared to one based upon geographic coordinates. This distortion will be particularly evident in the South Atlantic Anomaly (SAA), where the actual (offset) location of the dipole component of Earth's magnetic field is closest to Earth's surface.

The CGM coordinates for a given magnetic field model were provided to users in the form of a table for a uniform geographic coordinate grid (uniform spacing in latitude and longitude). Some of these tables were incomplete, and excluded low (CGM) latitudes. CGLALO incorporates such a table, using four point interpolation to compute the CGM coordinates except for the vicinity of the CGM poles where a three point interpolation method is used, with the CGM pole being one of the three points. The CGLALO_INVERSE routine computes geographic coordinates from CGM coordinates by using a search routine, and then performing a Newton-Ralphson procedure using the CGLALO routine. The current version of these two routines CGLALO95 and CGL95INV are based upon the IGRF 1995 Magnetic Field Model. To alleviate (and smooth) distortions in the vicinity of the magnetic equator, the IGRF 1995 tables used to generate CGLALO were modified as follows:

The magnetic dip equator is the set of points on the Earth reference sphere at which the actual magnetic field lines (as defined by the magnetic field model) are tangent to the sphere. Note that the dip equator does not actually lie in a plane, but is taken to be the reference plane (equator) for CGM coordinates. From the original tables, the entries within a band of ~15 degrees around the magnetic dip equator were deleted, and replaced by values obtained using a spline fit, with the added constraint that the spline curves pass through the coordinates of the dip equator.

The SFC_CONVERT_GEO_COORD routine computes Altitude Adjusted Corrected Geomagnetic Coordinates from Geographic Coordinates and altitude, and, where they exist, the inverse from CGM coordinates and altitude. In this enhancement of the CGM coordinate system concept, the CGM coordinates of an actual field line are constant for the portion of the field line north or south of the dip equator (at 0 km altitude). The CGM coordinates are the landing points of the field line, as defined by the CGLALO routine.

The original version was developed by *Baker and Wing* [1989] where the corrected geomagnetic coordinates (and the corresponding inverses) are computed by evaluation of functions for the X, Y, and Z components of a unit vector obtained from a spherical harmonic expansion. Since they were primarily interested with representing higher CGM latitudes, the South Atlantic Anomaly and the CGM equatorial region were not well represented. Subsequent versions are based upon an improved method described in *Bhavnani and Hein* [1994]. These versions were limited to an altitude range of 0-2000 km. The current version is based upon additional improvements described in *Hein and Bhavnani* [1996] has an altitude range of 0-7200 km. Versions of the current routine, and the CGLALO routines based upon the DGRF 1975, 1980, 1985, 1990 and IGRF 1995 models have been prepared for the research community.

Since the altitude adjusted CGM coordinates along a field line trace are (by definition) constant on a CGM hemisphere, and differ only by the sign of CGM latitude as they cross hemispheres, it is possible to use the current version (and, with less accuracy, previous versions) for field line tracing. A description of such usage and comparison with precision field line tracing routines are provided in *Hein and Bhavnani* [1996]. Table 16 provides a comparison of this usage with calculations using a precision magnetic field line tracing routine.

Table 16.

Comparison of Field Line Trace application of SFC_CONVERT_GEO_COORDINATE Routine with Precise Magnetic Field Line Trace.

Start Location for Trace			SFC CONVERT. output			PRECISE F.L. Trace output		
Altitude [km]	G.Lat. [deg]	G. Long. [deg]	Alt [km]	G.Lat. [deg]	G. Long. [deg]	G. Lat. [deg]	G. Lon. [deg]	Diff. [deg]
7200.0	30.000	.000	.0	55.938	355.040	55.288	355.300	.667
7200.0	30.000	30.000	.0	55.906	29.272	55.750	29.253	.157
7200.0	30.000	60.000	.0	55.358	60.747	55.298	60.693	.067
7200.0	30.000	90.000	.0	55.033	89.938	55.098	89.987	.071
7200.0	30.000	120.000	.0	55.769	118.530	55.765	118.512	.010
7200.0	30.000	150.000	.0	57.012	150.055	57.089	150.150	.093
7200.0	30.000	180.000	.0	56.040	185.768	56.099	185.812	.064
7200.0	30.000	210.000	.0	52.549	217.958	52.534	217.960	.014
7200.0	30.000	230.000	.0	50.208	236.728	50.184	236.657	.052
7200.0	30.000	270.000	.0	47.526	270.203	47.519	270.227	.018
7200.0	30.000	300.000	.0	48.448	294.408	48.655	294.484	.213
7200.0	30.000	330.000	.0	52.667	321.918	52.334	322.154	.363
7200.0	60.000	.000	.0	70.789	354.165	70.685	354.462	.143
7200.0	60.000	30.000	.0	71.284	28.946	71.073	29.236	.230
7200.0	60.000	60.000	.0	70.585	61.687	70.487	61.670	.098
7200.0	60.000	90.000	.0	69.963	90.753	69.980	90.893	.051
7200.0	60.000	120.000	.0	70.386	119.247	70.295	119.252	.091
7200.0	60.000	150.000	.0	71.149	150.897	71.110	150.630	.095
7200.0	60.000	180.000	.0	70.755	185.718	70.817	185.635	.067
7200.0	60.000	210.000	.0	68.741	217.917	68.851	218.055	.121
7200.0	60.000	230.000	.0	67.326	236.741	67.383	236.624	.073
7200.0	60.000	270.000	.0	65.770	269.499	65.949	269.466	.179
7200.0	60.000	300.000	.0	66.775	293.636	66.825	293.862	.102
7200.0	60.000	330.000	.0	68.985	321.455	68.907	321.661	.107
.0	50.000	.000	3600.0	33.782	1.955	33.817	1.988	.045
.0	50.000	30.000	3600.0	34.239	29.708	34.166	29.716	.073
.0	50.000	60.000	3600.0	35.133	59.033	35.172	59.055	.043
.0	50.000	90.000	3600.0	35.657	89.797	35.587	89.793	.071
.0	50.000	120.000	3600.0	34.549	121.489	34.513	121.449	.049
.0	50.000	150.000	3600.0	31.833	150.677	31.792	150.658	.044
.0	50.000	180.000	3600.0	32.461	177.091	32.609	177.099	.148
.0	50.000	210.000	3600.0	36.410	205.000	36.533	205.135	.164
.0	50.000	230.000	3600.0	39.188	225.403	39.205	225.518	.091
.0	50.000	270.000	3600.0	42.382	270.049	42.267	270.066	.116
.0	50.000	300.000	3600.0	40.750	304.276	40.645	304.160	.137
.0	50.000	330.000	3600.0	36.771	334.628	36.483	334.593	.289

The Diff. Field represents the difference along the arc of a great circle passing through the two points.

6. ATMOSPHERE/THERMOSPHERE MODELS

The models described in this section provide estimates of temperature, density and composition (neutral atoms and molecules) as a function of local time, day of year, altitude, geographic location, and geophysical conditions (solar and geomagnetic activity). Although the ionosphere lies within the model ranges, the free electron and ion content are not part of these models, but are described in the section on ionospheric models. References and sample test output for these models is provided.

6.1 MSIS Thermosphere Models

These models are empirical models based on mass spectrometer and incoherent scatter data - hence, the acronym MSIS. Mass spectrometer data, taken from instruments on board rockets and satellites, provides measurements of the number densities of the major constituents in the altitude range 100-700 km. Temperature data were taken from these satellites, as well as from rocket measurements between 85 and 300 km, and from ground based measurements of incoherent scatter at low altitudes (110-400 km) and at exospheric (above 500 km) altitudes.

The MSIS thermospheric models generate temperature and densities to an altitude of 1000 km, using analytic vertical temperature profiles. These temperature profiles depend on geographic coordinates, local time, day of year, and geophysical conditions (solar flux and geomagnetic activity). Vertical profiles of the densities are obtained from the temperature profiles as solutions of differential equations for diffusive and mixing equilibrium. In the mixing profiles, the densities of all constituents decay at the same rate with altitude, while in diffusive profiles, the decay rate depends on the molecular mass of the constituent (heavier ones decay more rapidly). The mixing profiles dominate below 105 km, and the diffusive profiles dominate above, with a smooth transition between the two regions.

The MSIS-83 empirical model [*Hedin*, 1983] was based on data from seven satellites and numerous rocket probes, as well as five ground based incoherent scatter stations. This model generated predictions of temperature, along with densities for N_2, O_2, O, He, Ar, and H. With the availability of temperature and composition measurements from the Dynamics Explorer B (DE-B), a revised version of the model was created, MSIS-86 [*Hedin*, 1987]. The DE-B data provided good coverage of the polar regions just after the peak of solar cycle 21, and suggested several refinements in the description of polar region morphology. Based on the DE-B data, plus data from Atmospheric Explorers C, D, and E, atomic nitrogen was added to the list of species. Both MSIS-83 and MSIS-86 had a low altitude limit near the mesopause (85 km).

The MSIS-90 thermospheric model [*Hedin*, 1991] revises MSIS-86 in the lower thermosphere and extends the model into the middle and lower atmosphere, providing a single analytic model of temperature and density profiles. This extension through the lower atmosphere is based mainly on tabulations from the <u>Middle Atmosphere Program (MAP) Handbook 16</u> by *Barnett and Corney* [1985]. Rocket and incoherent scatter data in the upper mesosphere and lower thermosphere have

also been incorporated in the revision. Latitude, annual, semiannual, and simplified local time and longitude variations are modeled using low-order spherical harmonics and Fourier series.

The sample MSIS-90 output shown in Table 17 was generated for 1994, with a geodetic latitude of 40°, and a longitude of 0°. Two solar flux and two geomagnetic activity cases are shown for each altitude/day/local time combination. Note that in addition to total mass density, the model can also compute the following:

- Number densities (per cm^3) for Ar, H, He, N, N_2, O, and O_2
- Exospheric temperature
- Temperature at given altitude

A test on a 66 MHz 486 PC making 10,000 calls to the MSIS-90 routine required 49 seconds; the same test ran in 40 seconds on a 40 MHz Sparc IPX workstation. A capability of using an extensive $a_p/F_{10.7}$ database also exists; this is useful when making "historical" model runs.

Table 17. Sample MSIS-90 Output

			$a_p = 7$ ($K_p = 2$)		$a_p = 48$ ($K_p = 5$)	
Alt	Day	LT	$F_{10.7} = 150$	$F_{10.7} = 220$	$F_{10.7} = 150$	$F_{10.7} = 220$
0	1	0	1.247E-03	1.237E-03	1.244E-03	1.243E-03
0	1	12	1.237E-03	1.237E-03	1.243E-03	1.242E-03
0	90	0	1.214E-03	1.215E-03	1.224E-03	1.223E-03
0	90	12	1.215E-03	1.215E-03	1.224E-03	1.223E-03
0	180	0	1.199E-03	1.200E-03	1.210E-03	1.209E-03
0	180	12	1.201E-03	1.201E-03	1.210E-03	1.209E-03
300	1	0	2.014E-14	3.789E-14	2.511E-14	4.565E-14
300	1	12	2.833E-14	5.236E-14	3.559E-14	6.364E-14
300	90	0	2.367E-14	4.213E-14	2.871E-14	4.919E-14
300	90	12	3.544E-14	6.180E-14	4.257E-14	7.176E-14
300	180	0	1.813E-14	3.301E-14	2.262E-14	3.915E-14
300	180	12	3.021E-14	5.295E-14	3.629E-14	6.098E-14
600	1	0	9.373E-17	3.165E-16	1.303E-16	4.231E-16
600	1	12	2.164E-16	7.696E-16	3.056E-16	1.031E-15
600	90	0	1.279E-16	4.168E-16	1.854E-16	5.576E-16
600	90	12	3.709E-16	1.226E-15	5.180E-16	1.584E-15
600	180	0	7.228E-17	2.560E-16	1.137E-16	3.560E-16
600	180	12	2.809E-16	9.687E-16	3.991E-16	1.243E-15

6.2 Groves/MSIS Atmospheric Model

The Groves/MSIS model is a hybrid, similar to the AFRA-86 model. The model is defined by a Global Reference Atmosphere [Groves, 1985] for altitudes from 18 to 70 km, and by the MSIS-83 thermospheric model above 130 km. A transitional model is used in the region between 70 and 130 km.

The Global Reference Atmosphere is derived from monthly means of zonal mean temperature, pressure, density, number density, and pressure scale height. These means have been tabulated at heights from 18 to 80 km, and latitudes from 80°S to 80°N, with a latitude interval of 10°. Monthly mean longitudinal variations of temperature, pressure, and density have also been tabulated for specific months in each hemisphere. The zonal means are derived from tabulations of temperature and geopotential height based on the following:

- Nimbus 5 SCR and Nimbus 6 PMR.
- A southern hemisphere reference atmosphere prepared for the 1984 COSPAR meeting in Graz, Austria, based on rocketsonde data.
- Two earlier northern hemisphere rocket-based reference atmospheres, CIRA-72 and the Air Force Reference Atmosphere 1978 (AFRA-78).

The longitudinal variations are derived solely from satellite based tabulations.

The transitional model [Groves, 1987] was designed to maintain continuity between the Global Reference Atmosphere and MSIS-83 in the second derivatives with respect to height of temperature, pressure, density, and constituent gas concentrations. In addition, a best fit is obtained to available temperature data, taken at 5 km steps from 75 km to 125 km. This temperature data consisted of that used for construction of CIRA-72, and rocket and incoherent scatter data presented at the 1984 COSPAR meeting in Graz, Austria. The transitional model was also designed to reproduce the required ratio of N_2 pressure at 70 km to that at 130 km, on integration of appropriate physical equations.

6.3 Jacchia Thermospheric Models

The Jacchia models [Jacchia, 1964; 1970; 1971; 1977] generate temperatures and densities using analytic vertical temperature profiles. These temperature profiles depend on geographic coordinates, local time, day of year, and geophysical conditions (solar flux and geomagnetic activity). Exospheric temperature is defined by these input parameters; the vertical profile is then determined from the exospheric temperature, with a geomagnetic activity dependent correction in the 1977 model.

The 1964 model generates profiles starting at 120 km, and is based primarily on satellite drag measurements. Analytic temperature profiles are generated based on fixed boundary conditions

31

at 120 km. These boundary conditions constitute a major drawback, since temperature and density undergo considerable variations at 120 km. The 1970 version is based on boundary conditions at 90 km, and contains a higher ratio of atomic-oxygen to molecular-oxygen density. Mixing of the various constituents (nitrogen, oxygen, argon, helium, and hydrogen) is assumed up to 105 km, with diffusion above this height. Moving the boundary to 90 km also required a change in the analytic expression used to generate the temperature profiles.

The 1970 model was approved for inclusion in the COSPAR International Reference Atmosphere (CIRA), subject to some suggested revisions. The molecular oxygen concentration was decreased further and that of atomic oxygen was increased, bringing the composition at 150 km in line with the results of a survey of experimental data. The transition from a condition of mixing of the various constituents to a state of diffusion was shifted to 100 km. This revised version of the Jacchia model was incorporated in CIRA [COSPAR, 1972], and is known separately as the Jacchia 1971 model.

The 1977 Jacchia model (J77) is based on satellite drag measurements taken from 1960 to 1975 above 200 km. In addition, the 1977 model incorporates mass spectrometer measurements from satellites OGO 6 and ESRO 4. An attempt is made to reproduce the results from OGO 6 for the relative concentrations of N_2 and O at 450 km, while keeping the total density profiles anchored to satellite drag. A similar approach was taken in the construction of the high altitude portion of the 1976 U.S. Standard Atmosphere [COESA, 1976]. Consequently, the J77 profiles at 1000 K are very similar to the U.S. Standard profiles, which are defined for an exospheric temperature of 1000 K.

Note that although the data coverage in altitude and composition is not as extensive as for the MSIS models, the solar activity reached a higher level during the data collection period than that reached during the cycle covered by most of the MSIS measurements. Therefore, the solar activity coverage of the Jacchia data is more extensive. A lack of flexibility in the vertical temperature profiles results in poor representation of variations with local time and geomagnetic activity. The Jacchia models lack a semidiurnal local time variation (two oscillations per day), normally seen at low altitudes but not at high altitudes. This is a result of using temperature profiles depending only on exospheric temperature (that is, high altitude data).

The sample Jacchia 77 output shown in Table 18 was generated for 1994, with a latitude of 40° and a longitude of 0°. Two solar flux and two geomagnetic activity cases are shown for each altitude/day/local time combination. A test on a 40 MHz Sparc IPX workstation making 10,000 calls to the Jacchia 77 routine required 21 seconds.

32

Table 18. Sample Jacchia 77 Output

			$a_p = 7$ ($K_p = 2$)		$a_p = 48$ ($K_p = 5$)	
Day	LT	Alt	$F_{10.7} = 150$	$F_{10.7} = 220$	$F_{10.7} = 150$	$F_{10.7} = 220$
1	0	100	5.832E-10	5.821E-10	6.340E-10	6.328E-10
1	12	100	5.821E-10	5.811E-10	6.328E-10	6.317E-10
90	0	100	6.278E-10	6.266E-10	6.833E-10	6.820E-10
90	12	100	6.272E-10	6.260E-10	6.826E-10	6.814E-10
180	0	100	5.528E-10	5.518E-10	6.021E-10	6.010E-10
180	12	100	5.519E-10	5.509E-10	6.012E-10	6.001E-10
1	0	300	1.724E-14	2.933E-14	1.833E-14	3.093E-14
1	12	300	2.515E-14	3.998E-14	2.662E-14	4.208E-14
90	0	300	2.495E-14	4.096E-14	2.695E-14	4.404E-14
90	12	300	3.401E-14	5.285E-14	3.668E-14	5.676E-14
180	0	300	1.938E-14	3.123E-14	2.124E-14	3.406E-14
180	12	300	2.544E-14	3.903E-14	2.784E-14	4.250E-14
1	0	600	7.437E-17	2.405E-16	8.305E-17	2.587E-16
1	12	600	1.675E-16	5.043E-16	1.850E-16	5.307E-16
90	0	600	1.568E-16	5.086E-16	1.771E-16	5.389E-16
90	12	600	3.253E-16	9.455E-16	3.564E-16	9.811E-16
180	0	600	1.165E-16	3.548E-16	1.289E-16	3.713E-16
180	12	600	2.204E-16	6.075E-16	2.376E-16	6.259E-16

6.4 Air Force Reference Atmosphere - 1986

The Air Force Reference Atmosphere (AFRA) [*Bass, et al.*, 1987] specifies temperature, pressure, and total mass density between 80 and 200 km. The AFRA model was derived by merging the MSIS-83 model (defined above 85 km) with a model of *Forbes* [1985], which is based on low altitude rocket and incoherent scatter measurements of temperature. The Forbes model is used in the lower portion of the AFRA altitude range, while MSIS-83 is used in the upper portion. A transition region provides a continuous and smooth match between the two models.

The Forbes model specifies monthly mean profiles of total mass density, temperature, and pressure between 65 and 120 km in tabular form. Temperature profiles were generated first by least squares fits to the data. The pressure profiles were obtained as solutions to the barometric equation, using the pressure at 68 km given by the AFRA-78 [*Cole, et al.*, 1978] as a lower boundary condition. The density is then derived from the perfect gas law.

The Forbes model depends only on altitude, latitude, and month, while MSIS-83 has additional dependencies on local time, solar activity, and geomagnetic activity. To determine the boundaries of the transition region, the additional dependencies were removed from MSIS-83. Comparisons of the two models showed a distinct disagreement between the two models, which worsened going from low to mid latitude. Therefore, it was concluded that the two models could not be brought

into agreement by a minor adjustment without compromising their validity in their separate regions of application.

The model definition that was adopted uses the Forbes model below 104 km and MSIS-83 above 120 km. A connecting model was defined for the region between 104 and 120 km. This connecting model computes the density, temperature, and molecular weight from cubic polynomials matching the Forbes model at 102 and 104 km, and matching MSIS-83 at 120 and 122 km. The pressure is then computed from the perfect gas law.

6.5 U.S. Standard Atmosphere 1976

The U.S. Standard Atmosphere, 1976 (US76) was adopted by the United States Committee on Extension to the Standard Atmosphere (COESA) in February, 1975 [1976]. This version is the same as the 1962 Standard Atmosphere below 50 km, but substitutes newer values at higher altitudes. COESA based the 1976 revision on the World Meteorological Organization's (WMO) definition of a standard atmosphere.

US76 is a steady-state representation of mean annual conditions of the atmosphere at a latitude of 45°N, defined for periods of moderate solar activity. The model is defined by sea-level temperature and pressure, and a temperature-height profile to 1000 km. The lower 32 km of the profile is identical to the International Civil Aviation Organization (ICAO) Standard Atmosphere. The portion between 32 and 55 km is based on radiosonde and meteorological rocketsonde observations. From 55 to 86 km, the model is based primarily on measurements from grenade, pitot static tube, and falling sphere experiments. Above 86 km, four functions are used that yield a continuous first derivative with respect to altitude over the entire region. These functions are based on various kinds of observational data [Jursa, 1985].

The basis for the 1976 revision is a much greater collection of experimental data, some over parts of the solar cycle not available for the 1962 version. Statistics compiled during preparation of the 1976 version showed that densities were about 10 percent lower in the 70 to 80 km region, and 10 percent higher in the 90 km region than those in the 1962 Standard. The 1976 version uses an exospheric temperature of 1000 K, compared to 1500 K in the 1962 model.

Presently, the US76 code will generate temperature, pressure, molecular weight, and total mass density up to 500 km. A test making 1,000,000 calls to the US76 routine required 24 seconds on a 40 MHz Sparc IPX workstation. A typical US76 density profile is shown in Table 19.

Table 19. Sample US76 Output

Alt (km)	Density (g/cm^3)	Temp (° K)	Pressure (dynes/cm^2)	Mole Wt (g/Mole)
100	5.604E-10	195.08	3.200E-01	28.40
150	2.076E-12	634.39	4.543E-03	24.10
200	2.541E-13	854.56	8.476E-04	21.30
250	6.073E-14	941.33	2.477E-04	19.19
300	1.916E-14	976.01	8.769E-05	17.73
350	7.014E-15	990.06	3.449E-05	16.74
400	2.803E-15	995.83	1.452E-05	15.98
450	1.184E-15	998.22	6.443E-06	15.25

The pressure values produced by the model code are calculated from the ideal gas law instead of the original tables; small differences due to round-off errors may occur.

6.6 Global Reference Atmospheric Model 1988

The Global Reference Atmospheric Model 1988 (GRAM88) is a hybrid consisting of three distinct zones and two transition regions [*Justus, et al*, 1980]. This model was developed by Georgia Tech, under NASA sponsorship. GRAM88 is valid over an altitude range of 0 to 700 km, and contains variations with latitude, longitude, and month. Table 20 summarizes the usage of the Jacchia 1970 and Groves 1971 models, and a 4-D atmospheric model developed for NASA by Allied Research Associates.

Table 20. GRAM88 Model Composition

```
                    Jacchia 1970
   115 ————————————————————————————
                    Transition between Jacchia and Groves models
    90 ————————————————————————————
                    Groves 1971
    30 ————————————————————————————
                    Interpolation between 4-D data and Groves model
    25 ————————————————————————————
                    NASA 4-D Model
Surface ————————————————————————————
```

The 4-D atmospheric model is based on empirically determined atmospheric parameter profiles taken at a large array of locations. This data consists of mean monthly and daily variance profiles of pressure, density, and temperature at 1 km intervals from the surface to 25 km, for the entire

35

globe. These data are interpolated over latitude and longitude to find the necessary values. In the transitional region from 25 to 30 km, an interpolation over height is performed between the NASA 4-D model and the Groves model.

The Groves 1971 empirical model combines many observations from a wide variety of longitudes, using observational results over a period of approximately 6 years. Latitude coverage of the Groves model is from the equator to 70° - 80°. Southern hemisphere data is taken as northern hemisphere data with a six month change of date. The Groves model data contains no longitude variation; rather, the data is modified by longitude, latitude, and height dependent stationary perturbations.

A smooth transition between the Groves and Jacchia models is obtained using a "fairing" technique, described by *Justus, et al.,* [1974]. This fairing is performed only at 95, 100, 105, and 110 km, which are the altitudes for which there are Groves values. The remaining locations in this transition region are then filled in using linear interpolation.

The sample GRAM-88 output shown in Table 21 was generated for 1994, with a geodetic latitude of 40°, and a longitude of 0°. Two solar flux and two geomagnetic activity cases are shown for each altitude/day/local time combination. A test run calculating 24 profiles, each containing three altitude points, required 288 seconds on a 40 MHz Sparc IPX workstation.

Table 21. Sample GRAM-88 Output

Alt	Day	LT	$a_p = 7$ $F_{10.7} = 150$	$(K_p = 2)$ $F_{10.7} = 220$	$a_p = 48$ $F_{10.7} = 150$	$(K_p = 5)$ $F_{10.7} = 220$
0	1	0	1.246E-03	1.246E-03	1.246E-03	1.246E-03
0	1	12	1.246E-03	1.246E-03	1.246E-03	1.246E-03
0	90	0	1.235E-03	1.235E-03	1.235E-03	1.235E-03
0	90	12	1.235E-03	1.235E-03	1.235E-03	1.235E-03
0	180	0	1.185E-03	1.185E-03	1.185E-03	1.185E-03
0	180	12	1.185E-03	1.185E-03	1.185E-03	1.185E-03
300	1	0	1.815E-14	2.396E-14	3.216E-14	3.831E-14
300	1	12	2.747E-14	3.362E-14	4.431E-14	5.011E-14
300	90	0	2.312E-14	2.918E-14	3.960E-14	4.559E-14
300	90	12	3.469E-14	4.081E-14	5.351E-14	5.881E-14
300	180	0	1.902E-14	2.488E-14	3.286E-14	3.900E-14
300	180	12	3.008E-14	3.624E-14	4.700E-14	5.267E-14
600	1	0	7.353E-17	1.410E-16	2.901E-16	4.517E-16
600	1	12	1.964E-16	3.243E-16	6.588E-16	9.135E-16
600	90	0	1.296E-16	2.280E-16	4.922E-16	7.101E-16
600	90	12	3.513E-16	5.317E-16	1.092E-15	1.420E-15
600	180	0	8.192E-17	1.546E-16	3.065E-16	4.733E-16
600	180	12	2.459E-16	3.924E-16	7.700E-16	1.046E-15

7. ORBITAL PREDICTION MODELS

Orbital prediction models provide the basis for the analysis of space-based observations of astronomical interest as well as Earth and near space environments. Where high precision is not required, orbital prediction based upon NORAD orbital elements, provided by SPACECOM and CSTC (SCF), are suitable for most purposes. The first of the orbital prediction models described here (LOKANGL) has been developed for use at Phillips Laboratory, and has been customized for use with a number of PL projects, in particular those involving Earth's magnetic field (ionosphere and magnetosphere). LOKANGL uses an analytic perturbation model. The second model is the standard Spacetrack package (SGP, SGP4, etc.) which implements five related analytic perturbation models. A comparison of LOKANGL with the Spacetrack models has been performed for several satellites pertinent to PL applications, with the finding that LOKANGL satisfactorily matches the recommended Spacetrack model (as determined by the satellite's orbital parameters).

To obtain higher precision than the LOKANGL and the Spacetrack models, it is usually necessary to implement a numerical integration scheme using a gravitational model (a spherical harmonic representation of Earth's gravitational field) and, for near earth satellites, an atmospheric density model, to compute the effect of drag. When tracking data are available, orbital parameters may be optimized using statistical weighting techniques.

The third model, ASAP, developed by JPL, provides this capability. At PL an adaptation of the ASAP program has been used to investigate lifetimes of satellites whose orbital decay is governed mostly by atmospheric drag. The latter is highly responsive to spatial and dynamical variations in the neutral density. Some of the density models used in these studies attempt to model variations due to solar-terrestrial effects due to extreme ultra violet (EUV) radiation and geomagnetic field heating due to charged particle precipitation.

Generally, the orbital elements provided by SPACECOM and CSTC are limited to the accuracy of the Spacetrack models. To obtain higher precision than these three models permit requires an orbital analysis package, which includes not only the capability to predict the position of a satellite, but also to compare predictions with actual observations, and perform differential correction, with either availability of such observations, or the capability and resources to make such observations.

7.1 LOKANGL Orbital Prediction Program

LOKANGL [*Hein, et al.*, 1991] is an orbit analysis and prediction program that has served broad requirements at Phillips Laboratory for many years. This program predicts the position and other orbital parameters of an Earth satellite using either NORAD or CSTC (SCF) orbital elements. LOKANGL also provides estimates of several important geophysical parameters at the location

of the satellite, such as L-shell value and dipole or corrected magnetic latitude and local time. In addition to the standard orbit prediction mode, LOKANGL employs an interpolation mode when generating an orbit that is bounded in time by a pair of successive element sets. Augmentation and adaptation of LOKANGL continues in response to various needs.

In the ideal case of two body motion, the orbit of two spherically symmetric masses bound by mutual gravitational attraction is an ellipse. However, for Earth satellites, deviations of Earth's mass distribution from spherical symmetry must be considered. LOKANGL models this deviation using an analytic perturbation technique, which takes into account the effect of the equatorial bulge and the north-south asymmetry.

In general, precision orbit prediction programs numerically integrate the equations of motion. By contrast, LOKANGL uses an analytic perturbation computation that is much more efficient in terms of computer time. This technique takes into account the second and third zonal harmonics of the Earth's gravitational field. Omission of the high order gravitational perturbation terms results in periodic errors of a few kilometers in-track within a single orbit. Other sources of error include the effect of atmospheric drag and lunar-solar perturbations. A study has been made to determine the effect of spacing of orbital elements on in-track errors [*Hein and Robinson*, 1991], and may be consulted for further information.

The major capabilities of LOKANGL are the following:

- Computation of a satellite's position and velocity vectors at regularly spaced time intervals.
- Calculation of a satellite's mean elements at regularly spaced time intervals.
- Determination of a satellite's position relative to as many as 20 stations located on the Earth's surface.
- Trajectory interpolation using pairs of orbital elements.
- Limited handling of orbital maneuvers is available.
- Modeling of atmospheric density/drag and geopotential for evaluating time derivatives of elements based on the method of King-Hele.
- Although not presently embedded in the program due to infrequent usage, a capability of providing look angles to satellites from moving stations (such as airplanes) is available.
- Calculation of solar illumination and shadowing of satellites.
- Options for printing a variety of output listings.
- A menu interface is available with the PC version of LOKANGL.

Table 22 gives position and velocity vectors for Mir over a 2-hour interval at 10-minute increments, while Table 23 presents sub-satellite data for the same time period. In a test on a 66 MHz 486 PC, calculation of sub-satellite data at 1-minute steps for a 5-day period required 50 seconds. Generation of position and velocity vectors over the same period required 42 seconds.

Table 22. Position and Velocity Vectors

SATELLITE 16609

DATE MO DY YR	U TIME HR MN SC	X(KM)	Y(KM)	Z(KM)	XDOT(KM/SEC)	YDOT(KM/SEC)	ZDOT(KM/SEC)
6 8 94	0 0 0	-3446.0984	2422.8861	-5314.7982	-4.575680	-6.141422	.169238
6 8 94	0 10 0	-5225.2233	-1521.4308	-4043.9981	-1.124580	-6.499486	3.904578
6 8 94	0 20 0	-4691.7660	-4791.4141	-979.2058	2.836488	-3.977076	5.916245
6 8 94	0 30 0	-2075.4085	-5933.4384	2520.8666	5.546864	.318820	5.296606
6 8 94	0 40 0	1463.5880	-4437.8990	4897.3146	5.792170	4.472043	2.317365
6 8 94	0 50 0	4352.8755	-971.1934	5092.8746	3.465825	6.635685	-1.690460
6 8 94	1 0 0	5309.8816	2926.5617	3021.4489	-.399898	5.853232	-4.946308
6 8 94	1 10 0	3908.8854	5524.6458	-395.4133	-4.088609	2.471850	-6.000387
6 8 94	1 20 0	773.1740	5671.7533	-3636.9303	-5.958497	-1.998035	-4.386461
6 8 94	1 30 0	-2705.4529	3309.2061	-5265.5130	-5.190155	-5.572081	-.833659
6 8 94	1 40 0	-4989.5734	-514.6431	-4562.6656	-2.129308	-6.683162	3.087027
6 8 94	1 50 0	-5067.0546	-4109.9947	-1837.0915	1.883670	-4.836818	5.647690
6 8 94	2 0 0	-2896.5254	-5881.0159	1705.0441	5.071887	-.836330	5.700232

Table 23. Sub-Satellite Output

SATELLITE 16609

DATE MO DY YR	U TIME HR MN SC	REV	GEOD LAT E	LONG	ALT(KM)	SZ ANG	SUNSH	LUNSH	LOCT	GMLAT	GMLONE	GMLT	L-SHELL	B/BO
6 8 94	0 0 0	47460	-51.775	-111.260	416.810	95.66	14.4	6.5	16.58	-43.23	326.75	17.32	1.944	9.16
6 8 94	0 10 0	47460	-36.789	-62.423	409.704	127.22	-17.2	-29.4	20.01	-26.26	7.69	20.21	1.344	1.75
6 8 94	0 20 0	47460	-8.360	-35.561	399.389	147.51	-37.8	-53.0	21.96	.33	35.05	22.19	1.143	1.06
6 8 94	0 30 0	47461	21.978	-12.949	397.386	135.06	-25.2	-27.8	23.64	27.27	62.34	.17	1.143	1.45
6 8 94	0 40 0	47461	46.523	22.075	402.155	104.91	5.1	8.3	2.14	44.93	103.95	3.10	1.931	9.44
6 8 94	0 50 0	47461	48.970	78.738	403.609	72.10	37.8	45.3	6.08	39.55	154.63	6.64	1.977	11.82
6 8 94	1 0 0	47461	26.634	117.671	400.230	42.71	67.1	80.2	8.84	16.11	188.10	9.03	1.112	1.71
6 8 94	1 10 0	47461	-3.365	141.022	401.100	33.37	76.5	85.8	10.57	-12.34	212.86	10.84	1.055	1.30
6 8 94	1 20 0	47461	-32.594	166.033	409.882	55.57	54.3	52.7	12.40	-37.87	243.63	13.05	1.783	8.38
6 8 94	1 30 0	47461	-51.108	-149.444	416.781	87.36	22.7	16.1	15.54	-47.87	293.52	16.53	2.506	23.34
6 8 94	1 40 0	47461	-42.470	-95.329	412.296	119.56	-9.5	-20.0	19.31	-32.65	338.88	19.71	1.470	3.15
6 8 94	1 50 0	47461	-15.821	-64.679	401.466	144.53	-34.7	-50.0	21.52	-5.25	6.15	21.69	1.143	1.04
6 8 94	2 0 0	47462	14.667	-42.453	396.924	140.75	-30.9	-36.2	23.17	23.93	30.43	23.46	1.211	1.66

7.2 Spacetrack Models for Propagation of NORAD Element Sets

The SPACETRACK code implements five different analytic perturbation schemes compatible with the NORAD satellite elements distributed by SPACECOM. The NORAD elements are mean elements which differ significantly from osculating (instantaneous position and velocity, or equivalent Keplerean elements) by modeling periodic perturbations due to deviations of Earth's gravitational field from spherical symmetry, and the effect of Earth's atmosphere upon satellite orbits. There is no "standard" definition of mean elements; each particular definition is characterized by the perturbations which are taken into account (modeled) and those which are ignored. The SPACETRACK codes enable users to make Position and Velocity predictions using the NORAD elements by using perturbation models which are compatible with the NORAD mean elements. The SPACETRACK code is described in the NORAD document "SPACETRACK REPORT #3 - Models for Propagation of NORAD Element Sets", December 1980.

According to the SPACETRACK report, the models recommended for element prediction are the SGP4 for near-earth satellites (orbital periods < 225 minutes) and SDP4 for longer period satellites. The latter model takes into account certain "resonance" terms in Earth's gravitational field for synchronous satellites, and for 12-hour period satellites, as well as perturbations due to the sun and moon. The SGP model is an older near-earth perturbation model that has been

replaced by SGP4. In addition to the SGP, SGP4 and SDP4 models, two additional models are available in SPACETRACK, SGP8 and SDP8, improved versions of SGP4 and SDP4, which, according to the document, have been proposed as replacements, but have not been officially adopted.

Program input consists of start and stop time, time interval in minutes (either forwards or backwards), followed by a two element set. Output is time (relative to epoch), and position vectors and velocity vectors (ECI) in [km], [km/sec].

Dr. Don Larson, SAIC has provided the following details:

NORAD elements are produced with SGP4, and are converted to the composite SGP/SGP4 2-line format to be fully compatible with the many SGP users (using the algorithms which have been supplied to thousands of requestors down through the years). The epoch time, eccentricity, inclination, right-ascension, argument of perigee, and mean anomaly terms are identical between SGP and SGP4. The SGP4 drag term (B-star) is included, as are the SGP drag terms (n-dot/2 and n-dot-dot/6). The mean motion listed is the SGP mean-mean-motion (that is, Kozai). It may be easily converted back to the SGP4 (that is, Brouwer) mean motion by removing the J2 (Kozai) term, via the algorithms alluded to above.

The earth model and physical constants are WGS-72, and the coordinate frame is: true equator and mean equinox of epoch (as listed on each element set), using the FK5 mean of J2000 time and reference frame.

7.3 ASAP - Artificial Satellite Analysis Program

ASAP is a satellite prediction program using precision numerical integration, developed by JPL for orbiting planetary spacecraft. It uses an eighth order Runge-Kutta-Fehlberg numerical integration routine with automatic step size control for the integration of the equations of motion to implement Cowell's method of special perturbations.

ASAP allows for the use of gravitational potential spherical harmonic expansions up to 40th order and degree, and optionally takes into account lunar and solar gravity, drag, solar radiation pressure (including planet shadow entry and exit). In addition to providing the US 1976 atmospheric density model for the Earth, it also allows for an exponential air density model for any planet. ASAP has been modified at PL to utilize dynamical atmospheric density models such as Jacchia 70 and MSISE 90.

In addition to the standard inputs (epoch [Ephemeris Time], and orbital elements of the spacecraft in either osculating or mean elements), option flags, and also model parameters, such as coefficients for spherical harmonics for gravitational potential fields, or geophysical indices for atmospheric density, must be provided by the user when options are selected.

40

References

Air Force Global Weather Central (1982), *AFGWC Polar Ionospheric Model*, Program Listing, Feb., 1982.

Anderson, D. N. (1973), A Theoretical Study of the Ionospheric F-region Equatorial Anomaly, II, Results in the American and Asian Sectors, *Planet. Space. Sci.,* **21**: 421-442.

Anderson, D. N., Mendillo, M., and Herniter, B. (1987), A Semiempirical, Low-latitude Ionospheric Model, *Radio Science,* **22**: 292-306.

Anderson, D. N., Forbes, J. M., and Codrescu, M. (1989), A Fully Analytic, Low- and Middle-Latitude Ionospheric Model, *J. Geophys. Res.,* **94** (A2): 1520-1524.

Baker, K. B. and Wing, S. (1989), A New Magnetic Coordinate System for Conjugate Studies at High Altitudes, *J. Geophys. Res.,* **94**: 9139.

Barghausen, A. L., Finney, J. W., Proctor, L. L., and Schultz, L. D. (1978), *Predicting Longterm Operational Parameters of High-frequency Sky-wave Telecommunications Systems*, ESSA Tech. Report, ERL 110-ITS 78.

Barnett, J. and Corney, M. (1985), Middle Atmosphere Reference Model Derived from Satellite Data, *Middle Atmosphere Program (MAP) Handbook 16*, Sci. Comm. for Solar-Terrestrial Physics Secr., University of Illinois, Urbana, IL.

Barraclough, D. R. (1987), International Geomagnetic Reference Field: the Fourth Generation, *Phys. Earth Planet. Inter.,* **48**: 279-292.

Barton, C. E. (1996), International Geomagnetic Reference Field Released, *EOS Trans.,* **77**(16): April 16.

Bass, J. N., Bhavnani, K. H., Bonito, N. A., Bryant, C. M. Jr., McNeil, W. J., Roberts, F. R., Sannerud, D. A., and Kantor, A. J. (1987), *Integrated Systems With Applications to the Multi-phases of the Ephemerides, Physics and Mathematics of the Upper Atmosphere*, Air Force Geophysics Laboratory Technical Report AFGL-TR-87-0064, ADA185748.

Bass, J. N. and Jordan, C. E. (1990), *Models of the External Source Contribution to Magneto-spheric Magnetic Fields For CRRES Data Analysis*, Geophysics Laboratory (AFMC) Technical Report GL-TR-90-0009, ADA221059.

Bhavnani, K. and Hein, C. A. (1994), *An Algorithm for Computing Altitude Dependent Corrected Geomagnetic Coordinates*, Phillips Laboratory Technical Report PL-TR-94-2310, ADA293967.

Bilitza, D. (1990), International Reference Ionosphere 1990, National Space Science Data Center, NSSDC/WDC-A-R&S 90-22, Greenbelt, Maryland.

Blake, J. B., Gussenhoven, M. S., Mullen, E. G., and Filius, R. W. (1992), Identification of an Unexpected Electron Space Radiation Hazard, *IEEE Trans. Nucl. Sci.*

Brautigam, D. H. and Bell, J. T. (1995), *CRRESELE Documentation*, Phillips Laboratory Technical Report PL-TR-95-2128, ADA301770.

Brautigam, D. H., Gussenhoven, M. S., and Hardy, D. A. (1991), A Statistical Study on the Effects of IMF, B_z, and Solar Wind Speed on Auroral Ion and Electron Precipitation, *J. Geophys. Res.*, **96**: 5525.

Chiu, Y. T. (1975), An Improved Phenomenological Model of Ionospheric Density, *J. Atmos. Terr. Phys.*, **37**: 1563-1570.

COESA (United States Committee on Extension to the Standard Atmosphere) (1976), *U.S. Standard Atmosphere, 1976*, U.S. Government Printing Office, Washington, D.C.

Committee on Space Research (COSPAR) (1972), *COSPAR International Reference Atmosphere*, Akademie-Verlag, Berlin.

Cole, A. E. and Kantor, A. J. (1978), *Air Force Reference Atmosphere*, Air Force Geophysics Laboratory Technical Report AFGL-TR-78-0051, ADA058505.

Coleman, C. J. (1993), *A General Purpose Ionospheric Ray Tracing Procedure*, Technical Report SRL-0131-TR, Defence Science and Technology Organisation (DSTO), Commonwealth of Australia.

Dandekar, B. S. (1982), *Ionospheric Modeling*, Air Force Geophysics Laboratory Technical Report AFGL-TR-82-0024, ADA115243.

Daniell, R. E., Jr., Brown, L. D., Anderson, D. N., Fox, M. W., Doherty, P. H., Decker, D. T., Sojka, J. J., and Schunk, R. W. (1995), PRISM: A Parameterized Real-Time Ionospheric Specification Model, *Radio Science*, **30**(5): 1499-1510.

42

Forbes, J. M.(1985), *Thermosphere Structure Variations During High Solar and Magnetic Activity Conditions*, Final Report, Air Force Geophysics Laboratory Technical Report AFGL-TR-86-0009, ADA171350.

Groves, G. V. (1985), *A Global Reference Atmosphere from 18 to 80 Km*, Air Force Geophysics Laboratory Technical Report AFGL-TR-85-0129, ADA162499.

Groves, G. V. (1987), *Modeling of Atmospheric Structure*, 70-130 Km, Air Force Geophysics Laboratory Technical Report AFGL-TR-87-0226, 1987, ADA201077.

Gussenhoven, M. S., Mullen, E. G., Sperry, M., Kerns, K. J., and Blake, J. B. (1992), The Effect of the March 1991 Storm on Accumulated Dose for Selected Satellite Orbits: CRRES Dose Models, *IEEE Trans. Nucl. Sci.*

Hardy, D. A., Hanser, F., and Sellers, B. (1985), The Space Radiation Dosimeter (AFGL-701-2), in *CRRES/SPACERAD Experiment Descriptions*, ed., M. S. Gussenhoven, Mullen, E. G., and Sagalyn, R. C., Air Force Geophysics Laboratory Technical Report AFGL-TR-85-0017, ADA160504.

Hardy, D. A., Gussenhoven, M. S., Raistrick, R., and McNeil, W. J. (1987), Statistical and Functional Representation of the Pattern of Auroral Energy Flux, Number Flux and Conductivity, *J. Geophys. Res.*, **92**: 12,275.

Hardy, D. A., Gussenhoven, M. S., and Brautigam, D. (1989), A Statistical Model of Auroral Ion Precipitation, *J. Geophys. Res.*, **94**: 370.

Hardy, D. A., McNeil, W. J., Gussenhoven, M. S., and Brautigam, D. (1991), A Statistical Model of Auroral Ion Precipitation 2. Functional Representation of the Average Patterns, *J. Geophys. Res.*, **96**: 5539.

Hedin, A. E. (1983), A Revised Thermospheric Model Based on Mass Spectrometer and Incoherent Scatter Data: MSIS-83, *J. Geophys. Res.*, **88**(A12): 10,170-10,188.

Hedin, A. E. (1987), MSIS-86 Thermospheric Model, *J. Geophys. Res.*, **92**(A5): 4649-4662.

Hedin, A. E. (1991), Extension of the MSIS Thermosphere Model into the Middle and Lower Atmosphere, *J. Geophys. Res.*, **96**(A2): 1159-1172.

Hein, C. A. and Bhavnani, K. (1996), *An Expanded Algorithm for Computing Altitude Dependent Corrected Geomagnetic Coordinates*, Phillips Laboratory Technical Report PL-TR-96-2274, ADA324654.

Hein, C. A., Bhavnani, K. H., and Robinson, E. C. (1991), *Private Communication.*

43

Hein, C. A. and Robinson, E. C. (1991), *Private Communication.*

Hilmer, R. V. (1989), *A Magnetospheric Magnetic Field Model with Flexible Internal Current Systems*, Ph. D. thesis, Rice Univ., Houston, Tex.

Hilmer, R. V. and Voigt, G. H.(1995), A Magnetospheric Magnetic Field Model with Flexible Current Systems Driven by Independent Physical Parameters, *J. Geophys. Res.*, **100**(A4): 5613.

Jacchia, L. G. (1964), *Static Diffusion Models of the Upper Atmosphere with Empirical Temperature Profiles*, Smithsonian Astrophysical Observatory Special Report No. 170.

Jacchia, L. G. (1970), *New Static Models of the Thermosphere and Exosphere with Empirical Temperature Profiles*, Smithsonian Astrophysical Observatory Special Report No. 313.

Jacchia, L. G. (1971), *Revised Static Models of the Thermosphere and Exosphere with Empirical Temperature Profiles*, Smithsonian Astrophysical Observatory Special Report No. 332.

Jacchia, L. G. (1977), *Thermospheric Temperature, Density, and Composition: New Models*, Smithsonian Astrophysical Observatory Special Report No. 375.

Jasperse, J. R. (1982), The Photoelectron Distribution Function in the Terrestrial Ionosphere, *Physics of Space Plasmas*, ed. by T.S. Chang, B. Coppi, and J.R. Jasperse, Scientific Publishers, Cambridge, MA, pp. 53-84.

Jordan, C. E.(1989), *NASA Radiation Belt Models AP-8 and AE-8*, Geophysics Laboratory (AFMC) Technical Report GL-TR-89-0267, ADA223660.

Jursa, A. S., Sci. Editor (1985), *Handbook of Geophysics and the Space Environment*, Air Force Geophysics Laboratory Technical Report AFGL-TR-85-0315, ADA167000.

Justus, C. G., Woodrum, A., Roper, R. G., and Smith, O. E. (1974), *A Global Scale Engineering Atmospheric Model for Surface to Orbital Altitudes, 1: Technical Description*, NASA-TM-X-64871.

Justus, C. G., Fletcher, G. R., Gramlink, F. E., and Pace, W. B. (1980), *The NASA/MSFC Global Reference Atmospheric Model - MOD 3 (With Spherical Harmonic Wind Model)*, NASA Contractor Report 3256.

Kerns, K. J. and Gussenhoven, M. S. (1992), *CRRESRAD Documentation*, Phillips Laboratory Technical Report PL-TR-92-2201, ADA256673.

Kluge, G. (1972), Direct Computation of the Magnetic Shell Parameter, *Computer Phys. Communications*, **3**: 31-35.

Langel, R. A. (1991), International Geomagnetic Reference Field, 1991 Revision, *J. Geomag. Geolectr.*, **43**: 1007-1012.

Langel, R. A. and Estes, R. H. (1985), The Near-Earth Magnetic Field at 1980 Determined from MAGSAT Data, *J. Geophys. Res.*, **90**: 2495-2509.

Langel, R. A., Barraclough, D. R., Kerridge, D. J., Golovkov, V. P., Sabaka, T. J., and. Estes, R. H (1988), Definitive IGRF Models for 1945, 1950, 1955, and 1960 , *J. Geomag. Geoelectr.*, **40**: 645-702.

Lloyd, J. L., Haydon, G. W., Lucas, D. L., and Teters, L. R. (1978), *Estimating the Performance of Telecommunication Systems Using the Ionospheric Transmission Channel* (4 volumes), National Telecommunications and Information Administration, Boulder, Colorado.

Lynch, K., Boughan, E., Fischi, D., Hardy, D., Riehl, K. (1989), *PROTEL: Design, Fabrication, Calibration, Testing and Satellite Integration of a Proton Telescope*, Air Force Geophysics Laboratory Technical Report AFGL-TR-89-0045, Environmental Papers, # 337, ADA214564.

McIlwain, C. E. (1961), Coordinates for Mapping the Distribution of Magnetically Trapped Particles, *J. Geophys. Res.*, **66**: 3681.

Meffert, J. D. and Gussenhoven, M. S. (1994), *CRRESPRO Documentation*, Phillips Laboratory Technical Report PL-TR-94-2218, ADA284578.

Millman, G. H., Bowser, C. A., and Swanson, R. W. (1988), An Ionospheric Model for HF Sky Wave Backscatter Radar, pp. 43-1 to 43-15, *AGARD Conference Proceedings No. 441*, NATO-AGARD Symposium on 'Ionospheric Structure and Variability on a Global Scale and Interactions with Atmosphere, Magnetosphere', Munich, Federal Republic of Germany, May 16-20.

Morel, P. R., Hanser, F., Sellers, B., Hunerwadel, H., Cohen, R., Kane, B. D., and Dichter, B. K. (1989), *Fabricate, Calibrate, and Test a Dosimeter for Integration into the CRRES Satellite*, Air Force Geophysics Laboratory Technical Report AFGL-TR-89-0152, ADA213812.

Mullen, E. G., Gussenhoven, M. S., Ray, K., and Violet, M. (1991), A Double-Peaked Inner Radiation Belt: Cause and Effect Seen on CRRES, *IEEE Trans. Nucl. Sci.*, **38**: 1713.

Olson, W. P. and Pfitzer, K. A. (1977), *Magnetospheric Magnetic Field Modeling, Annual Scientific Report*, AFOSR Contract No. F44620-75-C-0033, McDonnell Douglas Astronautics Company, Huntington Beach, CA.

Sawyer, D. M., and Vette, J. I. (1976), A*P-8 Trapped Proton Environment for Solar Maximum and Solar Minimum*, NSSDC/WDC-A-R&S 76-06.

Schunk, R. W. (1988), A Mathematical Model of the Middle and High Latitude Ionosphere, *Pure Appl. Phys.*, **127**: 255-303.

Spjeldvik, W. N. and Rothwell, P. L. (1985), The Radiation Belts, Chap. 5 in *Handbook of Geophysics and the Space Environment*, ed., A. S. Jursa, Air Force Geophysics Laboratory Technical Report AFGL-TR-85-0315, ADA167000.

Tsyganenko, N. A. (1987), Global Quantitative Models of the Geomagnetic Field in the Cislunar Magnetosphere for Different Disturbance Levels, *Planet. Space Sci.*, **35**(11): 1347-1358.

Tsyganenko, N. A. and Usmanov, A. V. (1982), Determination of the Magnetospheric Current System Parameters and Development of Experimental Geomagnetic Field Models Based on Data from IMP and HEOS Satellites, *Planet. Space Sci.*, **30**(10): 985-998.

Violet, M. D., Lynch, K., Redus, R., Riehl, K., Boughan, K., Hein, C. (1993), The Proton Telescope (PROTEL) on the CRRES Spacecraft, *IEEE Trans. Nucl. Sci.*, **40**: 242.

Voigt, G. H. (1981), A Mathematical Magnetospheric Field Model with Independent Physical Parameters, *Planet. Space Sci.*, **29**: 1.

Whartenby, W. G. (1993), PIM User's Guide, Version 1.0.6, Computational Physics, Inc., Newton, MA; draft version, June 2.